UCRL-19096

c. 2

THE INTERACTION OF HIGH FREQUENCY ELECTROMAGNETIC RADIATION OF SUPERCONDUCTING POINT CONTACT JUNCTIONS

Stewart Allen Sterling
(Ph. D. Thesis)

RECEIVED
LAWRENCE
RADIATION LABORATORY

MAR 5 1970

LIBRARY AND
DOCUMENTS SECTION

December 1969

AEC Contract No. W-7405-eng-48

TWO-WEEK LOAN COPY

This is a Library Circulating Copy
which may be borrowed for two weeks.
For a personal retention copy, call
Tech. Info. Division, Ext. 5545

LAWRENCE RADIATION LABORATORY
UNIVERSITY of CALIFORNIA BERKELEY

UCRL-19096 c.2

34

DISCLAIMER

This document was prepared as an account of work sponsored by the United States Government. While this document is believed to contain correct information, neither the United States Government nor any agency thereof, nor the Regents of the University of California, nor any of their employees, makes any warranty, express or implied, or assumes any legal responsibility for the accuracy, completeness, or usefulness of any information, apparatus, product, or process disclosed, or represents that its use would not infringe privately owned rights. Reference herein to any specific commercial product, process, or service by its trade name, trademark, manufacturer, or otherwise, does not necessarily constitute or imply its endorsement, recommendation, or favoring by the United States Government or any agency thereof, or the Regents of the University of California. The views and opinions of authors expressed herein do not necessarily state or reflect those of the United States Government or any agency thereof or the Regents of the University of California.

TABLE OF CONTENTS

ABSTRACT v

I. INTRODUCTION 1

II. SUPERCONDUCTIVITY AND THE JOSEPHSON EFFECT 3

A. Properties of Bulk Superconductors 3

B. The Josephson Effect 5

C. Weak Links 10

III. POINT CONTACT JOSEPHSON JUNCTIONS 12

A. Coupling Radiation to Josephson Junctions 12

B. Current-Voltage Characteristics of Point Contact Junctions 14

C. Detection 17

IV. EXPERIMENTAL TECHNIQUES 21

A. Spectroscopic Techniques 21

1. Radiation Source 21

2. Fourier Transform Spectroscopy 21

3. Detector Linearity 23

4. Narrowband Response Interferograms 25

B. Sample Preparation 26

1. Sample Materials 26

2. Sample Mounting 26

3. Fabrication 28

4. Sample Adjustment 29

C. Resonators 29

D. Electrical Measurements 30

E. Cryogenics 32

V. RESONANT DETECTION 34

A. Undriven Self-Induced Step 35

B. Driven Self Induced Step 40

1. Non-resonant Detection 40

2. Resonant Detection 41

C. Zero Voltage Detection 45

VI. EXPERIMENTAL RESULTS 47

A. Resonant Detection 47

1. Noise Equivalent Power 50

2. Detector Noise 53

B. Multiple Junction Effects 54
1. Apparatus 55
2. Results 56
C. Broadband Response 59

APPENDIX A - The Derivation of Josephson Effect 62
APPENDIX B - Energy Conservation in the ac Josephson Effect 65
APPENDIX C - Corrections to the WS Theory 67

ACKNOWLEDGEMENTS 71
REFERENCES 72
FIGURE CAPTIONS 75
FIGURES 78

THE INTERACTION OF HIGH FREQUENCY ELECTROMAGNETIC RADIATION OF SUPERCONDUCTING POINT CONTACT JUNCTIONS

Stewart Allen Sterling

Department of Physics, University of California
and
Inorganic Materials Research Division,
Lawrence Radiation Laboratory,
Berkeley, California 94720

ABSTRACT

Experimental evidence is presented on the interaction of millimeter and submillimeter electromagnetic radiation with point contact Josephson junctions. Changes in the dc current voltage characteristic are used to measure changes in ac Josephson currents coupled to radiation fields, and the detection properties of such junctions are discussed in detail. Evidence is presented for feedback narrowed response when the ac Josephson currents are strongly coupled to a resonant cavity. The observed response shows high sensitivity (NEP $\lesssim 5\times10^{-15}$ W/$\sqrt{\text{Hz}}$) and frequency selectivity ($Q_{eff} \gtrsim 10^3$). The Werthamer-Shapiro theory has been extended to include the effects of applied radiation at the resonance frequency and is shown to account for the feedback narrowing. In addition, evidence for the frequency dependence for the ac currents is presented.

I. INTRODUCTION

Point contact junctions between two superconductors coated with a natural oxide show many properties characteristic of thin film tunnel junctions. These include both quasiparticle and Josephson tunneling currents. The earliest reported applications of such junctions were as dc interferometers.[1] Because point contact junctions are more easily coupled to electromagnetic radiation than thin films, more recent applications have been for ac effects.[2] Grimes, Richards and Shapiro (GRS)[3,4] have investigated the use of point contact junctions as detectors of electromagnetic radiation. They demonstrated that point contacts can detect radiation up to frequencies well above the two-particle energy gap. Additionally, their measurements of spectral response are characterized by considerable structure, some of which they attribute to the frequency dependence of the ac Josephson current.

GRS also demonstrated that point contact junctions showed the ac Josephson effect when driven at frequencies as high at 32.2 cm^{-1}, observing the constant voltage currents steps generated by coherent radiation from a cyanide far infrared laser. Grimes and Shapiro[5] showed that point contact junctions could be used to mix two applied frequencies, generating detectable difference frequencies. Parker et al.[6] have used point contact junctions (as well as thin films) to make precise measurements of $\hbar/2e$. Silver and Zimerman[7] have demonstrated that point contacts coupled to a resonant circuit may be used to do absorption spectroscopy over a wide frequency range.

Point contact junctions have generated considerable interest as detectors of millimeter and submillimeter waves. The best existing detectors are liquid helium cooled bolometers, whose noise-equivalent-powers can

be as low at 10^{-12} watt/$\sqrt{\text{Hz}}$. GRS have demonstrated that point contact detectors are an order of magnitude more sensitive and further are characterized by very fast response times. In this thesis we will describe further results on point contact detection of far infrared radiation. Both broadband and resonant detection (narrow band) will be described, we will consider, in general, the effect of high frequency electromagnetic radiation on the dc current voltage properties of point contact junctions. Any such change can be used for detection. We will consider in some detail the coupling of a point contact junction to a resonant cavity and will describe a very sensitive, narrow band detection mechanism.[8] In addition we will use the spectral response of point contact junctions to study some of the high frequency ac Josephson effects.

The organization of this thesis is as follows: In Section II we briefly sketch some of the properties of bulk superconductors and the Josephson effect. In Section III we discuss the properties of point contact junctions and how they affect our detection experiments. In Section IV we describe our experimental techniques and apparatus. In Section V we discuss the coupling of the ac Josephson current to a resonant structure and detection effects arising from such coupling. In Section VI we discuss the results of our experiments on resonance coupled detectors as well as attempts to make broad band response measurements.

II. SUPERCONDUCTIVITY AND THE JOSEPHSON EFFECT

A. Properties of Bulk Superconductors

Properties of bulk superconductors are well known:[9] at temperatures below a transition temperature T_c, certain materials exhibit a state of zero dc resistance[10] and perfect diamagnetism (Meissner Effect)[11]. In the absence of an applied magnetic field the transition to the superconducting state is a second order thermodynamic transition characterized by a discontinuity in specific heat. In 1935, F. and H. London[12] observed that one could explain the Meissner Effect by assuming that the superconducting state is characterized by a single many-body wave function which is unperturbed by weak electromagnetic fields. The resulting absence of a paramagnetic contribution to supercurrents in a sample implies the observed flux exclusion. London[13] further showed that in a multiconnected sample, magnetic flux trapped by the superconductor is quantized. To account for the thermodynamic properties of superconductors, Gorter and Casimer[14] postulated a two-fluid model whereby a temperature dependent fraction of electrons in a system condense into a superfluid state for $T < T_c$. By assuming that the "normal" fluid contributed a quadratic temperature dependence to the free energy, they were able to predict the gross thermodynamic features of superconductivity.

In 1950, Ginsberg and Landau[15] proposed a major extension of the theory of the electrodynamics of superconductors. They proposed that the superconductor be characterized by an order parameter, $\psi(\vec{r})$, whose square modulus is proportional to the number of superconducting electrons. Near the transition temperature, they expanded the free energy of the superconducting system in a power series of $|\psi(\vec{r})|^2$. By assuming that $\psi(\vec{r})$ was such that it minimized the free energy of the system, they

derived the magnetic behavior of superconductors. Although only valid for a limited temperature range near T_c the Landau-Ginsberg theory has proved very useful where electromagnetic fields cannot be treated as perturbations on the zero field superconducting wavefunction. To include London's "rigid" wave function ideas, they included in the free energy a gauge-invariant, term proportional to $|\vec{\nabla}\psi - i \frac{e}{\hbar c} \vec{A} \psi|^2$ which forced spatial variations in the order parameter to increase the total free energy.

In 1957 Bardeen, Cooper and Schrieffer (BCS)[16] presented the first successful microscopic theory of superconductivity. They pointed out that, given a weak attractive electron-electron interaction, the electronic free energy favors a condensation of part of the electron gas into a state composed of time-reversed electronic states. At a temperature $T < T_c$, these pair states have an energy lower than the unpaired states by a nonzero energy gap, $\Delta(T)$. They constructed the "BCS model," based on an isotropic attractive interaction which was nonzero only over a finite energy range around the Fermi energy. The model relates the zero temperature energy gap to the transition temperature by $\Delta(0) = 1.76\ kT_c$ and predicts a $\Delta(T/T_c)$ curve tabulated by Muhlschegel.[17]

Gor'kov,[18] using the BCS theory, derived the Landau-Ginsberg theory showing that the order parameter $\psi(\vec{r})$ was proportional to the energy gap Δ, and that the charge in the Landau-Ginsberg theory was twice the electronic charge.

The existence of an energy gap has been demonstrated repeatedly, verifying the general features of the BCS model.[19] Measurements of the low temperature specific heat of superconductors gave the first, indirect evidence of the gap, and the surface impedance studies first showed directly the lack of electron states below the gap. Perhaps the most informative technique for gap measurements was introduced by

Giaever in 1960. He observed non-linearities in the current-voltage characteristic of a superconductor-insulator-superconductor junction which were easily interpretable in terms of an energy gap. Quasi-particles can tunnel through the insulating layer only if they start from occupied states and end in unoccupied states. In a superconductor at T=0, all of the electrons are in the condensed state and one can pass a quasi-particle current between the superconductors only when the voltage bias across the insulating layer is large enough so that the ground state of one superconductor has the same energy as the empty quasi-particle continuum of the other. Experimentally, the junction carries no current until the voltage equals $2\Delta(0)/e$ (the factor of two arises from the paired nature of the condensed state. Two electrons must simultaneously tunnel across the insulator, each requiring an energy Δ.) At nonzero temperatures thermal excitations of quasi-particles into the continuum above the gap smear the gap edge on the current voltage characteristic, although the gap can still easily be measured as the minimum in the differential resistance versus voltage characteristic. Tunneling measurements have verified that the density of quasi-particle states is zero below Δ, peaks sharply at Δ, and approaches the normal metal density of states above Δ. (The BCS model predicts that the distribution of excited states is derived from $E = [\Delta^2 + \epsilon^2]^{1/2}$, where E is the quasi-particle energy corresponding to the normal metal state ϵ.)

B. The Josephson Effect

In 1962 Josephson[21] pointed out that superconducting pairs can tunnel across the insulating barrier at zero voltage. This Josephson current contributes a resistanceless current step at V=0 with a magnitude at T=0 of up to $I_1 = \pi/R \frac{\Delta_1 \Delta_2}{\Delta_1+\Delta_2}$ where the subscripts refer to the

two superconductors making up the junction, and R is the normal-state junction resistance; further Josephson predicted that at non-zero voltages the supercurrent could alternate with a frequency given by $2eV_{dc}/\hbar$, [$2e/\hbar$ = 483.6 MHz/μV.]

Consider two superconductors separated by an insulating barrier (usually the oxide of one of the superconductors). The insulator is thin enough that there may be an observable tunneling current and thick enough that the interaction between the superconductors can be treated to the lowest order in the tunneling hamiltonian. In Appendix A we show that there is a term in the energy of the system favoring the coupling of the superconducting wave functions. If we represent the superconducting wavefunction by $\psi(\vec{r},t) = \psi_0(\vec{r})\, e^{i\psi(t)}$, then the interaction energy per junction area has the form

$$\Delta E = \frac{\hbar j_i}{2e} \cos\left(\phi_1 - \phi_2 - \frac{2e}{\hbar c}\int_1^2 \vec{A}\cdot d\vec{\ell}\right) \quad (1)$$

where the line integral is taken across the insulating barrier. Further, the current density through the insulator is $j = j_i \sin\left(\phi_1 - \phi_2 - \frac{2e}{\hbar e}\int_1^2 \vec{A}\cdot d\vec{\ell}\right)$. (We will use j_1 for the amplitude of Josephson current density and I_1 for the total amplitude of the current, thus averaging over spatial variations.)

The equation of motion for the phase difference across the insulating layer can be derived from the time dependence of the wave function. For a superconductor in equilibrium, its wave function satisfies the time-dependent Schroedinger equation: $H\psi = i\hbar\, \partial\psi/\partial t$, so $\psi = \psi(r) \exp(-iEt/\hbar)$. Gor'kov[18] showed that according to the BCS theory, $E = 2\mu$, i.e. the change in Gibbs free energy when two electrons are used to add a another superconducting particle (a Cooper pair) to the system represented by $\psi(r,t)$. If each of the superconductors comprising the junction is in equilibrium, then $\partial\phi_i/\partial t = 2\mu_i/\hbar$ and $\partial(\phi_1-\phi_2)/\partial t = +2(\mu_2-\mu_1)/\hbar$.

If we apply a small (time-dependent) voltage across the junction, departures from local equilibrium may be neglected and the chemical potential difference becomes eV(t), thus

$$\frac{\partial}{\partial t}(\phi_1-\phi_2) = \frac{2eV(t)}{\hbar} \tag{2}$$

One effect of the presence of $\vec{A}$ in (1) is to require the Josephson current to screen out applied magnetic fields. Josephson showed that this screening current implies a magnetic penetration length $\lambda_J = [\hbar c^2/8\pi e\, j_1 d]^{1/2}$ where d is the magnetic thickness of the junction, equal to the penetration depths of each superconductor plus the barrier thickness. Typically this junction penetration is on the order of one millimeter.

For small enough junctions the magnetic field penetrates the junction area uniformly. For example, for a magnetic field, H, parallel to the length (L) of a uniform junction, the vector potential term in (1) becomes $2ed/\hbar c\, Hx$, where x is the spatial coordinate along L. Now the current density in the junction of width w, is

$$j(x) = j_1 \sin(\Delta\phi - \frac{2ed}{\hbar c} Hx) \tag{3}$$

and the total current through the junction is

$$I = w \int_{-L/2}^{L/2} j(x)\, dx$$

$$I = j_1 wL \frac{\sin\pi\, \Phi/\Phi_0}{\pi\, \Phi/\Phi_0} \sin\Delta\phi \equiv I_1(H) \sin\Delta\phi \tag{4}$$

where $\Phi/\Phi_0 = edL/\hbar c\, H$ and $\Phi_0 = hc/ie$ is the flux quantum. The constant $\Delta\phi$ is determined by the biasing circuit, and the junction can carry a maximum dc current of $I_1(H)$. The dc Josephson Effect, this interference of supercurrents, was first observed by Anderson and Rowell.[23] They observed that the critical current, $I_1(H)$ carried by a Josephson junction oscillated with magnetic field according to the predicted

$|\sin x/x|$ single slit diffraction pattern.

Equation (2) shows that if there is a non-zero voltage across the junction, then the phase difference increases linearly in time, and the Josephson current alternates as $I(t) = I_1 \sin(\omega_0 t + \phi_0)$ where ϕ_0 is an arbitrary constant and $\omega_0 = 2e\, V_{dc}/\hbar$ and V_{dc} = voltage bias. Thus the junction carries no dc current for $V \neq 0$. Josephson suggested that the ac Josephson current can be observed by imposing an ac voltage across the junction in addition to the dc voltage. For $V(t) = V_{dc} + V_{rf} \cos(\omega_{rf} t + \phi_{rf})$, the junction current is

$$I = I_1 \sin\left[\omega_0 t + \xi_{rf} \sin(\omega_{rf} t + \phi_{rf}) + \phi_0\right]$$

or

$$I = I_1 \sum_{N=-\infty}^{\infty} J_n(\xi_{rf}) \sin\left[(\omega_0 + n\omega_{rf})\, t + \phi_0 + n\phi_{rf}\right] \qquad (5)$$

where $J_n(\xi_{rf})$ is an nth order Bessel function of the first kind and $\xi_{rf} = 2e\, V_{rf}/\hbar\omega_{rf}$. Now (5) will have a frequency component at dc when $\omega_0 = N\omega_{rf}$. Under these conditions the junction will pass a dc current at a series of equally spaced voltages, the voltage separation being $\Delta V = \hbar\omega_{rf}/2$ and the amplitude of the steps is given by $|2I_1 J_N(\xi_{rf})|$. This effect was first measured by Shapiro.[24] Note that now the dc phase across the junction is $\phi_0 + N\phi_{rf}$ and one observes a maximum current step when $\phi_0 + N\phi_{rf} = \pi/2$.

If there is an ac voltage across the junction, the ac Josephson current may radiate detectable coherent electromagnetic radiation. In Appendix B, we show that the simple voltage-biased Josephson junction conserves energy. The power radiated by the ac current equals the dc power supplied by the bias circuit. Typically, the junction current is coupled to a resonant circuit, and the ac current in the junction induces an ac voltage in the resonant circuit, which induces an ac voltage across

the junction. Radiation emitted by junction-resonator system have been observed in a number of types of resonators: the resonant strip line cavity formed by the insulating junction barrier and superconducting sides of an evaporate film junction,[25] point contact junctions in microwave cavities,[26] and point contact junctions coupled to radio frequency circuit.[27]

Ambegaokar and Baratoff,[22] have calculated the amplitude of the dc Josephson current at nonzero temperatures using the method of thermodynamic Green's function. They find that for identical superconductors obeying the BCS model, $j_1 = \frac{\pi}{2R}\Delta(T)\tanh[\frac{1}{2\beta}\Delta(T)]$ where R is the normal state resistance of the junction, $\Delta(T)$ is the energy gap at T and $\beta = [kT]^{-1}$. As T approaches the transition temperature, the Josephson current goes linearly to zero.

More recently, Werthamer[29] extended the calculation of Ambegaokar and Baratoff to include the ac Josephson current. He found that in the BCS model, as Riedel[30] has pointed out earlier, the amplitude of the ac current has a logrithmic singularity $\omega_0 = (\Delta_1+\Delta_2)/2$. He found that in the presence of an ac voltage across the junction, the Josephson current should be represented by

$$I(t) = \mathrm{Im}\left\{ e^{i\phi_0} \sum_{n,n'} J_n J_{n'} j_2(n\omega_{rf} - \tfrac{1}{2}\omega_0) \times \exp i[(n+n')\omega_{rf}t - i\omega_0 t] \right\} \qquad (6)$$

where $j_2(\omega)$ is the complex temperature dependent Josephson current with a singularity at $\omega = \Delta_1 + \Delta_2$. J_n and $J_{n'}$ are Bessel functions of argument $\frac{1}{2}\xi_{rf}$ and the sum runs over all integers n and n'. The singularity arises from the singular density of states in the BCS model at $\Delta_1+\Delta_2$. In practice this singularity is certainly rounded by gap anisotropies and Cooper pair lifetimes. The functional dependence of the real

observable part of $j_2(\omega)$ is shown in Fig. 1. The function actually plotted is $j(\omega) = \frac{1}{2}\,\mathrm{Re}\ \{j_2(\omega) + j_2(0)\}$ which we shall show later to be the predicted Josephson junction response to low-level radiation at frequency ω.

C. Weak Links

Josephson[31] and Anderson[32] have both pointed out that (2) is very general. The phase slippage relationship in a superconductor applies equally well to two superconductors separated by a weak link (a small constriction) or to a single superconductor. Equation (2) may be considered the equation defining the existence of a non-zero voltage across a superconductor.

Anderson and Dayem[33] have demonstrated that a single superconducting weak link between two superconductors exhibits properties similar to the ac Josephson effect. They irradiated a weak link junction with microwaves and observed constant voltage steps on the dc current voltage characteristic. The device supported constant voltage steps at $V_{dc} = n\hbar\omega_{rf}/2me$ where n and m are integers; that is, the microwaves induced both harmonic and subharmonic steps. In contrast, a Josephson junction will support only harmonic steps. Additionally, the weak link step amplitudes do not oscillate with microwave power as do the Josephson steps (see Eq. (5)).

The ac (finite voltage) effects exhibited by weak links is attributed to the motion of fluxoids across the link. One can show that the line integral of $\nabla\phi$ around a fluxoid is 2π, and so when ever a fluxoid crosses the weak line the relative phase changes by 2π. The existence of a non-zero voltage, V_{dc} requires that $(2e\,V_{dc}/\hbar)$ fluxoids cross the link per unit time. When microwave power is applied to the link, the fluxoid

motion through the link is synchronized with the applied rf fields, and the weak link will support a constant voltage step whenever m fluxoids cross the link every n cycles of the microwave field.

Mercereau[34] has demonstrated that weak links, as well as Josephson junctions, connected by a loop of bulk superconductors exhibit supercurrent interference. The applied magnetic flux through the loop determines the phase change across each link. The total critical current of the system depends on the magnitude of the circulating supercurrent. For two identical junctions enclosing a total flux Φ in the area betweem them, the critical current of the system can be shown to be proportional to $\cos(\pi\Phi/\Phi_0)$ where Φ_0 is the flux quantum.

III. POINT CONTACT JOSEPHSON JUNCTIONS

In this section we discuss some of the properties of point contact junctions and the advantages of such junctions over thin film junctions as detectors of high frequency radiations: their relatively high rf impedance allows efficient coupling to electromagnetic radiation; their continuous dc current-voltage characteristics provide a sensitive mechanism for detecting changes in supercurrent amplitudes. We consider the physical origins of these properties.

A. Coupling Radiation to Josephson Junctions

The conventional method for fabricating high quality Josephson junctions is the vacuum evaporation of thin films. One strip is deposited on a substrate, the strip is allowed to oxidize and a second strip is deposited over the first. With careful preparation, such a junction will show nearly ideal Josephson behavior; that is, its maximum dc supercurrent is within a few percent of the theoretical value and displays the predicted $|\sin x/x|$ diffraction pattern in a magnetic field. Thin film junctions however are large parallel plate capacitors with a plate of separation of only a few Angstroms. For frequencies of interest to us, i.e. in the far infrared, the capacitance of thin film junctions presents an extremely low impedance to the electromagnetic radiation. A junction with an area of 1 mm^2 and an insulating layer of 10Å has a capacitance on the order of 0.01 μf. For 10 cm^{-1} radiation (=300 GHz) the rf impedance of such a capacitance is $\sim 5\times10^{-5}$ ohms. Typically the junction is coupled to a microwave transmission system whose characteristic impedence is on the order of tens or hundreds of ohms. The rf voltage transmitted to the junction from the line is reduced by approximately the ratio of the impedances i.e., by a factor of 10^6 or 10^7. This problem is considered in detail later.

This impedance mismatch problem is reduced by decreasing the junction capacitance, while holding the maximum Josephson current constant. The capacitance is proportional to the junction cross-section, while inversely proportional to its thickness. The Josephson current is also proportional to the cross-sectional area, but is exponentially dependent on insulating layer thickness.[35] (The tunneling matrix elements determining the Josephson current amplitude depend on the spatial overlap of electronic wavefunctions across the insulator.) One, then, reduces the barrier thickness slightly and the cross-sectional area by orders of magnitude.

The standard solution is to fabricate junctions in a point contact geometry. One superconductor, in the form of a wire, is sharpened to a point and pressed against the flat face of a second superconductor. The thermally grown oxide layer on both superconductors provides the insulating barrier. Typically, the oxide layers are elastic and deform under pressure, so the thickness of the insulating layer may be controlled by controlling the contact force between the two superconductors. The superconducting wire may be easily sharpened to a point whose radius of curvature is a few microns giving typical junction areas of $\approx 10^{-4} - 10^{-6}$ mm^2.

The physical scale of interest for Josephson junctions is the barrier thickness-- on the order of a few Angstroms. On this scale the sharp point is expected to be quite rough and contacts may be formed in several places. Further some of these contacts may form weak links, where the superconductor has punctured through the oxide layer. We expect, then, that a point contact junction will be composed of several Josephson junctions and weak links in parallel. Figure 2 shows an idealized microscopic contact where part of the current is carried by tunneling and part by metal-to-metal contact.

As stated above, weak links are known to show Josephson-like behavior: They can carry a zero voltage current up to some critical current, then make a continuous transition to a resistive state at non-zero voltage, due presumably to flux flow across the link. In addition, parallel weak links, like parallel Josephson junctions, exhibit interference of supercurrents in a magnetic field. The distinguishing feature between them is that in a microwave field, a weak link will support subharmonic as well as harmonic steps. Further, weak link steps do not oscillate in height as the microwave power is increased. We use these ac properties (generation of constant voltage steps) to determine whether a point contact is primarily weak link of Josephson. Our experiments are on point contacts that are essentially the latter.

B. Current-Voltage Characteristics of Point Contact Junctions

The shunting impedence provided by weak links in the resistive state and ohmic shorts in a point contact determines the current voltage characteristic of the Josephson junctions. We have shown that at non-zero dc voltage biases the Josephson current does not contribute to the dc current. McCumber[36] demonstrated that the presence of a shunting impedence requires the junction to carry a dc current for $V \neq 0$. He showed that the I-V characteristic of a point contact junction can be explained if the Josephson junction is shunted by an ohmic conductance, while that of a thin film junction is due to a shunting capacitance. We consider the former as it pertains to our experiment. The effect of the shunt conductance is to make the voltage across the junction a single-valued, monotomic function of current.

Assume that the point contact can be represented by an ideal Josephson junction shunted by a conductance, G, the system being driven by a

constant current I. The constant current drive implies that the ac currents in the junction also pass through the conductance, generating ac voltages which appear across both the conductance and the junction which, in turn, generate dc currents in the junction. Specifically, the current through the junction is $I_J(t) = I_1 \sin\phi$, where $\frac{\partial\phi}{\partial t} = 2eV(t)/\hbar$ and through the conductance is $I_G = GV = \frac{\hbar G}{2e}\frac{\partial\phi}{\partial t}$. Using $I_j + I_0 = I$,

$$I_1 \sin\phi + \frac{\hbar G}{2e}\frac{\partial\phi}{\partial t} = I$$

$$\frac{\hbar G}{2eI}\frac{d\phi}{dt} + \frac{I_1}{I}\sin\phi = 1 \tag{7}$$

Solving for $\phi(t)$, and remembering that $V_{dc} = \frac{2e}{\hbar}\overline{d\phi/dt}$, we get

$$V_{dc} = \begin{cases} 0\,, & I < I_1 \\ G^{-1}\sqrt{I^2 - I_1^2}\,, & I > I_1 \end{cases} \tag{8}$$

The upper curve in Fig. 3 shows this characteristic. Several points should be emphasized: (i) the curve is continuous. By sweeping the constant current bias, we can trace out all of the dc system voltages. (ii) the height of the zero voltage critical current is unaffected by the shunting conductance. (iii) the differential resistance of the junction for non-zero voltages goes to $1/G$ as $V \to \infty$ and to ∞ as $V \to 0$. This last feature will prove important to our detection mechanism. This model agrees with experiment for point contacts whose shunt capacitance does not contribute to the total impedances i.e., when the capacitive impedance at frequencies of interest ($\sim 2e\,V_{dc}/\hbar$) is much larger than G^{-1}. (For high dc voltages the differences between various types of shunt impedance becomes negligible, since $V_{dc} \to I/G$, and quasi-particle currents become important.) Note that at non-zero voltage biases, the constant current source delivers power to the Josephson junction. That is the

junction carries a non-zero dc current at a non-zero voltage. One can show that this power is dissipated in the conductance as an ac power generated by the junction, in contrast to a Josephson junction in a microwave field, where the dc power delivered to the junction contributes to the microwave field.

The existence of thermal noise modifies the current-voltage characteristic discussed above. Ambegaokar and Halperin[37] showed that thermal current fluctuations in a point contact (Josephson junction plus shunt conductance) round the transition from the super-current state at V=0 to the resistive state at $V \neq 0$, removing the singular differential resistance at V=0. Physically, the rounding is due to a partial decoupling of the phases of the two superconductors. We show in Appendix I that the energy favoring phase coupling is given by $\Delta E = \hbar I_1/2e \cos \Delta\phi$ ($\hbar/2e \simeq 2°K/\mu A$). If the thermal noise in the point contact is greater than this coupling energy ΔE, then the Josephson effect is unobservable. Since the junction current is given by $I_1 \sin \Delta\phi$, for $I \sim I_1$ the coupling energy is small and the phases begin to decouple. Ambegaokar and Halperin show the significant rounding occurs for $\hbar I_1/2e \sim 40$ kT.

In Fig. 4 we show the current-voltage characteristic of a tantalum-tantalum point contact. It shows many of the features we have considered. The point contact has a critical current of about 65μA rounded a bit by, presumably, thermal noise. The characteristic is continuous, with a high differential resistance near V=0 and a well-defined gap edge at ±1.1 m V. The effective noise temperature seen by the junction is somewhere between the point contact temperature and room temperature. The biasing circuit, composed of a battery in series with a large resistor generates thermal noise with T = 300°K. But much of this noise is filtered out by a low temperature filter shunting the point contact. The minimum noise temperature is the junction temperature. The low degree of rounding

of the critical current in Fig. 4 indicates that the effective noise temperature is near the bath temperature.

C. Detection

We have defined a detector to be a device which gives a dc response to an applied electromagnetic field. Equation (5) gives the direct current response of a Josephson junction to a monochromatic rf voltage. Whenever $\omega_0 = N\omega_{rf}$ the junction carries a dc current of $I_1 J_N(\xi_{rf}) \sin(\phi_0 - N\phi_{rf})$. Such a junction can thus serve as a detector. In a point contact, these induced current steps are typically superimposed on I-V characteristic, connected to the resistive part of the characteristic by regions of high differential resistances similar to those discussed for the zero voltage step.

The junction response to a small change in applied rf voltage is given by the change in height of the induced rf step; viz: $\Delta I \simeq I_1 J_N'(\xi_{rf}) \Delta\xi_{rf}$, where $J_n'(x) = d J_n/dx$. (Since we are monitoring the maximum step current, $\sin(\phi_0 - N\phi_{rf}) = 1$.) The change in the current step height is monitored by biasing the point contact with a constant current to the high differential resistant region near the step. As the step height changes, the high differential resistance follows it, and the dc bias voltage changes.

In our experiments we measure the junction response to very low-level far infrared signals. In this case $\xi_{rf} \ll 1$, and so $\Delta I \cong I_1 J_N'(0)\, \xi_{rf}$. Only the first step (N=1) responds linearly to the applied rf voltage. The first step, however, has zero height at these small power levels and so has no high differential resistance on which to bias. More important, one can show that any thermal noise will round a step of infinitesimal height completely[37] making it unobservable. Only the N=0 step will be observable. The response of the N=0 step is, to lowest order, quadratic

in ξ_{rf}, since $J_0'(0) = 0$; i.e. $\Delta I \cong -1/4\ I_1\ (\xi_{rf}^2)$. (9)

The junction can be used as a detector linear in ξ_{rf} by using a superheterodyne technique. That is, apply sufficient rf power from a local oscillator so that the Nth current step is easily resolved over thermal rounding. If a low-level signal voltage is applied, the total rf voltage across the junction is $\xi_{LO} \sin(\omega_{LO}t) + \xi_{rf} \sin(\omega_{rf}t)$, where ξ_{rf} is the signal voltage and ω_{LO} and ω_{rf} are the local oscillator and signal frequencies respectively. To lowest order in ξ_{rf} the rf voltage can be expressed as $[\xi_{LO} + \xi_{rf} \cos(\omega_{LO} - \omega_{rf})t] \sin(\omega_{LO} + 1/2\ \omega_{rf})t$. If $N\omega_{LO} \simeq \omega_{rf}$, then the junction current response is $\Delta I = I_1\ J_N'(\xi_{LO})\ \xi_{rf} \cos(\omega_{LO} - \omega_{rf})t$. The Nth step then oscillates at the difference frequency with an amplitude ξ_{rf}. This detection scheme has been used by Grimes and Shapiro.[5]

The actual detector signal (the change in dc voltage bias) depends sensitively on the dc junction characteristic and on the bias used. When biased to a region of high differential resistance, the junction voltage is sensitive to small changes in current. From (5), the voltage response to a change in the zero voltage critical current is

$$R(V_{dc}) = + \frac{I_1}{G^2\ V_{dc}}, \tag{10}$$

where $R(V)$, the junction responsivity, is defined to be $-\ dV_{dc}/dI_1$ for constant I. The singular responsivity at V=0 is removed by the thermal rounding of the critical current. Equation (10) is the lower curve in Fig. 3. The signal from the detector is now $V_s \equiv \Delta V = R(V_{dc})\Delta I$.

The junction response to low-level far infrared radiation is, from (9)

$$V_s = R(V_{dc})\ (\xi_{rf}^2)/4 \tag{11}$$

In deriving (11) we have neglected the frequency dependence of the ac Josephson current predicted by Werthamer.[29] We should have begun our discussion using (6) instead of (5). Our arguments need to be altered by considering I_1 to be a function of the applied rf frequency. From (6) we can show that the response of the zero voltage critical current should be written

$$V_s = j(\omega)\, R(V) \quad (\xi_{L_{rf}}{}^2)/4 \tag{12}$$

where $j(\omega)$ is plotted in Fig. 1.

Further frequency dependences to (12) enter when we consider the coupling between the junction and the microwave transmission line carrying the rf power from the source. Due to the impedance mismatch between the junction and transmission line, the induced rf voltage is related to the applied voltage by some coupling constant $\Gamma_R(\omega)$. Using the fact that the square of applied rf voltage is proportional to the applied power $S(\omega)$ and $\xi_{rf} \propto V_{rf}/\omega$, we have

$$V_s \propto j(\omega)\, \Gamma_R(\omega)\, R(V)\, S(\omega)/\omega^2 \tag{13}$$

Typically the frequency dependence in $\Gamma_R(\omega)$ dominates the frequency response of the point contacts. A comparison of (12) and (13) shows that Γ_R is proportional to $\xi_{rf}{}^2/S(\omega)$. According to simple transmission line theory

$$\frac{V_{rf}{}^2}{S(\omega)} = \frac{4\, Z_J{}^2\, Z_0}{(Z_J+Z_0)^2} \tag{14}$$

where Z_J and Z_0 are the impedences of the point contact and the transmission line respectively, the transmission line impedance is close to that of free space (377Ω) since the far infrared radiation is being carried by an oversized wave guide. The point contact impedance is more difficult to estimate. Its low frequency impedance ($\omega \sim \frac{2eV_{dc}}{\hbar}$, less than a few cm^{-1})

is essentially ohmic, since the observed I-V characteristics agree with McCumber's model of a point contact. Its high frequency impedance is not known but is probably capacitive, accounting for the observed high frequency roll-off of the junction response.

Most of the frequency dependence of Γ_R is due to resonances in the surroundings of the point contact. The metallic surfaces (e.g. superconductors themselves, waveguide, point contact holders, etc.) are all of a size comparable to a radiation wavelength of interest (~ 1mm). The resonances included by these surfaces act as impedance transformers, matching the far infrared transmission line to the point contact. Their effect is to give a large frequency dependence to the effective values of the impedances in (14). Treating the point contact and metallic surfaces as a resonator terminating the far infrared transmission line, the rf voltage induced across the junction depends on both the impedance matching of the resonator to the transmission line and the resonator fields at Z_J. Changing Z_J changes both the resonator field across the junction and impedance that the resonator presents to the transmission line.

IV. EXPERIMENTAL TECHNIQUES

A. Spectroscopic Techniques

1. Radiation Source

The source of far infrared radiation used in our experiments was a laminar grating interferometer, described by Barker,[38] modified to work in the aperiodic mode.[39] The broad band black body radiation from a General Electric UA-3 mercury-arc lamp was focused by f/1.5 optics onto a laminar grating and then through a low-pass filter onto the point contact detector. The radiation was chopped at 33 Hz to allow for coherent detection of the detector signal. Without low pass filtering, the modulated output of the interferometer extended to 80 cm^{-1}. The low frequency ($\nu < 25$ cm^{-1}) power spectrum is approximately the Rayleigh-Jeans black body distribution with about 5×10^{-10} watts/cm^{-1} of power at 10 cm^{-1}. That is with frequency measured in cm^{-1}, $S(\nu) \simeq 5\times10^{-12}\ \nu^2$ watt/cm^{-1}.

2. Fourier Transform Spectroscopy

We measured the spectral response of the point contact junctions using the techniques of Fourier transform spectroscopy.[39] The speed of data acquisition, high resolution, lack of "false energy" problems, and adequate signal-to-noise ratios make this technique more advantageous than using a monochrometer. We present a brief description of the technique to acquaint the reader with its advantages and limitations.

Collimated broad band radiation is split into two beams, one of which travels a distance Δ further than the other. (In our case, half of the radiation is reflected off the front half of the laminar grating and half off the back.) The beams are recombined, chopped and transmitted via a 1.1 cm i.d. light pipe to the detector. If the spectral intensity of the beam falling on half of the grating is $S(\nu)$, the total modulated output

intensity is

$$\Phi(\Delta) = \int_0^\infty d\nu \quad S(\nu)\cos 2\pi\nu\Delta \tag{15}$$

This power, $\Phi(\Delta)$, falls on the point contact detector and a signal voltage is recorded as a function of path difference Δ. In particular, if the detector signal is proportional to the applied spectral power density, then the detected signal $\Phi(\Delta)$ (called the interferogram) is

$$\Phi(\Delta) = \int_0^\infty d\nu \; S(\nu)\; R(\nu) \;\; \cos 2\pi\nu\Delta \tag{16}$$

where $R(\nu)$ is the system response to unit power at a frequency ν. Given the complete interferogram, $\phi(\Delta)$, for all $\Delta \geq 0$, we can calculate $R(\nu)$ using the Fourier transform theorem to invert Eq. (16)

$$R(\nu) = \frac{4}{S(\nu)} \int_0^\infty d\Delta \; \Phi\;(\Delta) \;\cos 2\pi\nu\Delta \tag{17}$$

In practice one measures $\Phi(\Delta)$ at regular, discrete, intervals ($\Delta = n\Delta_0$) and truncates the interferogram after reaching some $\Delta_{max} = N\Delta_0$. The resultant interferogram is inverted via (17) by a high speed digital computer. The calculated spectral response is

$$R_{obs}\;(\nu) = \frac{4\Delta_0}{S(\nu)} \sum_{n=1}^{N} \Phi\;(n\Delta_o)\;\cos\;(2\pi\nu n\Delta_0) \tag{18}$$

The approximations to $\Phi(\Delta)$ result in two limitations on our spectral response results: (i) the discrete sampling of the interferogram places a high frequency limits on the calculated spectral response of $\nu_{max} = 1/2\Delta_0$. Response to any higher frequency, ν', appears as false energy at $\nu = n\,\nu_{max} - \nu'$ where n is such that $0 < \nu < \nu_{max}$. For example, if $\Delta_0 = 0.25$ mm the contribution of radiation at 25 cm^{-1} will appear on the computed spectral response at 15 cm (= 2×20-25). Proper selection of low pass filtering eliminates this problem.

(ii) Truncation of $\Phi(\Delta)$ limits the spectral resolution. One can show that the number of significant spectral points obtainable from (18)

equals the number of data points, N. One can circumvent this only by continuing the interferogram far enough out in Δ to include all significant information.

The most significant advantage of this technique is the enhancement of signal-to-noise ratio on the computed spectrum. If the noise on the detector signal is independent of signal, then one can show that in spectrum of N points, the spectral noise is reduced by $\sqrt{N/2}$ compared to the interferogram noise. This noise reduction is due to each spectral points being a weighted average of all N interferogram points.

In addition, the problem of filtering is reduced to one of finding a single low-pass filter which removes radiation for $\nu > \nu_c$. In our experiments, the filtering problem is eliminated by the natural high frequency cut-off of the spectral response of junctions.

The disadvantages of the technique are due to two features: (i) the data are not obtained in an easily interpretable form, being the Fourier transform of the spectral response in which we are interested; and (ii) many frequencies are simultaneously incident on the detector. The former is a drawback because transforming the data requires the availability of a digital complex, although the raw data becomes at least partially understandable with experience. The latter is, for our experiments, more serious. Josephson junctions are well known to be efficient mixers of rf signals, and yet the assumption that the junction signal is proportional to the power incident on it is fundamental to the interpreting of the interferogram. In the next section we consider the effects of such mixing.

3. Detector Linearity

The non-linearities inherent in Josephson effect devices offer several possible detector deviations from the assumed square law response. In

Section II we showed that the zero voltage current response is proportional to $J_0(\xi_{rf})$ and that for $\xi_{rf} \ll 1$ the response is quadratic in ξ_{rf}. The effects of higher powers of ξ_{rf} can be understood in the following way: Assume that in addition to the quadratic dependence, the response also depends on ξ_{rf}^4, i.e. proportional to $[S(\nu)]^2$. The square law term gives the undistorted spectral response, while the additional term introduces harmonics. That is, the interferogram, defined in (15), will have a nonlinear contribution proportional to $[S(\nu) \cos 2\pi\nu\Delta]^2$ due to the higher order response at frequency ν. Where the interferogram is Fourier transformed this contribution appears as spectral emergy at 2ν. The most obvious way to determine this existence of such saturation phenomena is to record a series of interferograms with a series of neutral filters in the far infrared beam, and ratio the resulting spectral responses. Any differences between various sets of data must be due to higher order responses. An easier method however, involves using the fact that most of our spectral response curves show well defined, high Q, structure. If the junction is saturating, this structure will appear also at harmonics e.g., a peak at ν_1 will also appear at $2\nu_I$. Such harmonic structure was never seen in our data.

The mixing of two far infrared frequencies is expected to be on the same order as the above deviations from square law behavior. The response of the critical current to two different frequencies can be shown to be proportional to $J_0(\xi_1) J_0(\xi_2)$ where $\xi_{1,2}$ are the rf amplitudes. For $\xi_{1,2} \ll 1$, this becomes $1 - 1/4\,(\xi_1^2 + \xi_2^2) + 1/64\,(\xi_1^4 + \xi_2^4 + 4\xi_1^2\,\xi_2^2)$. The mixing terms are the same order as the non linearity we discussed above and are not believed to contribute.

If the actual voltage across the junction is non-zero, mixing of infrared and Josephson frequencies may be detected. For a given ω_0

the junction will carry dc currents whenever the frequency of the applied radiation equals a harmonic of the Josephson frequency. Detection of such dc currents is equivalent to detecting microwave induced steps at finite voltages. The power output of the interferometer is so small that any steps generated are probably smeared by thermal noise.[37] Experimentally we have observed no dependence of the spectral response on the voltage bias of the junction when biased to monitor the zero voltage current.

4. Narrowband Response Interferograms

We often observe response peaks that are much narrower than the resolution width of the interferometer (0.2 cm^{-1}). If such a narrow peak dominates the interferogram, we may estimate its linewidth by fitting the interferogram to the Fourier transform of a Lorentzian line shape. That is, let $R(\nu) = R_0(\nu_0)[1 + (\pi/\Delta\nu)^2 (\nu-\nu_0)^2]^{-1}$ where ν_0 and $\Delta\nu$ are the peak frequency and line width respectively. If the spectral power $S(\nu)$ is constant over the frequency range of interest, then the interferogram is

$$I(\Delta) = I_0 e^{-\Delta/\lambda} \cos (2\pi\nu_0\Delta) \tag{19}$$

where $\lambda = 1/2\Delta\nu$ and is the decay length of the envelope modulating the cosine. An example is given in Fig 5, where we have plotted the detector signal against the path difference. With a bit of calculation we find that $\lambda \cong 1.8$ cm, so $\Delta\nu = 0.28$ cm^{-1}. The peak frequency occurs at $\nu_0 =$ 0.28 cm^{-1}. This interferogram was taken with $\Delta_0 = 0.1$ mm, giving $\nu_c =$ 50 cm^{-1}. Had we measured it out to the 5 cm path difference, the sharp peak in the spectrum would be described by only 3 or 4 points. If we are interested in the line shape, we can analyze the interferogram differently. In Fig. 5 we have recorded it on a fine enough scale that we can extract the envelope by hand, getting about 50 points ranging from

$\Delta = 0$ to $\Delta = 30$ mm. Analytically, the Fourier transform of this envelope $g(\Delta)$ gives the line shape $g(\nu-\nu_0)$ and we calculate ν_0 from the interferogram directly.

B. Sample Preparation

1. Sample Materials

We used both niobium and tantalum wires to form point contact junctions. Both materials were of unknown purity although we observed that tantalum point contact junctions typically could carry supercurrents below a transition temperature of 4.25 - 4.30°K (the accepted value for pure Ta is $T_c = 4.38°K$). Both materials were easy to machine and sharpen, though the niobium was malleable and could be bent quite easily. We used niobium for experiments not directly involving the measurement of gap properties, since at 4.2°K it shows essentially its T = 0°K superconducting properties. Tantalum was used when gap effects were under consideration since 95% of its zero temperature gap could be reached by pumping on the helium bath.

We attempted to fabricate point contacts out of lead on lead and lead on niobium, in order to take advantage of the plastic properties of lead. Lead posts with niobium points were easy to fabricate and showed good ac Josephson effects but they were not particularily sensitive to far infrared radiation.

2. Sample Mounting

We developed a sample holder which allowed precise positioning of the point against the post and yet was sufficiently rigid to reduce microphonics to negligible proportions. The point contact junctions characteristic was still senstive enough to vibration that it could be changed by gently tapping the dewar top but stable enough to survive the vibrations associated

with the advancing of the interferometer path difference mechanism and repeated temperature cycling between 4.2 and 1.2°K.

The holder is shown in Fig. 6. The frame is machined from aluminum into the form of a yoke, with the side arms machined to a cross section of a "U" beam, to minimize arm mass while maintaining arm rigidity. The arms of the yoke are compressed by the nuts (N), controlled by the position of the differential screw (D). To prevent the nuts from binding the differential screw as the yoke arms compress, the nuts are mounted on pivoting pins. The position of the differential screw is controlled from the dewar top via a worm gear (not shown) driving the spur gear attached to the screw. The differential screw, with 20 and 24 threads/inch, had a travel sufficient to contract the yoke arms by about 1.2 millimeters.

The superconducting wires (S_1,S_2) held in place in bakelite insulators (I) fastened to the arms of the yoke. The superconducting wires are secured in the insulators by opposed screws (C), one of which is not shown, to which the electrical contacts are soldered. One of the wires (S_2) is bent in the shape shown to provide a spring pushing the two wires together with constant force. As the yoke arms are compressed, the spring in S_2 is compressed, increasing the force compressing the natural elasticity of the oxide layer on the superconductors. In this fashion the thickness of the insulating barrier separating the superconductors can be accurately controlled. The natural vibrational frequencies of the points contacts has been made high ($\approx$ 8 KHz) compared with laboratory vibrations by (i) having as small a mass as possible suspended by the loop in S_2 and (ii) making the yoke arms as rigid as possible. The great frequency difference between the point contact vibrational frequencies and ordinary laboratory vibrations is enough to decouple the junction from most shocks and vibrations.

The far infrared radiation transmitted from the interferometer down light pipe (L), a 1.1 cm brass tube whose wall thickness has been reduced to 1/4 mm to reduce thermal conduction into the helium bath. The light pipe also provides the mechanical support for the yoke. The radiation is focused by a cone onto the junction. As shown, the radiation is not confined to the region of the junction in order to eliminate geometric resonances which dominate the spectral response of point contact junctions in most geometrics (see Sec. VI). Resonant cavities, discussed below, can be attached to the light pipe or to one arm of the yoke when studying the effects of strongly coupled resonator modes on junction properties.

3. Fabrication

The points were fabricated from a short (~2 cm) section of superconducting wire of up to 0.75 mm in diameter. The wire was first mechanically sharpened with a file and then with No. 400 emery cloth. The tip of the sharpened point was then inspected under a 40 power microscope. Before being set aside to oxidize, the tip was etched for a few seconds in a solution of 5 parts concentrated HNO_3, 4 parts concentrated HF and 1 part CH_3COOH and rinsed in distilled water and clean isopropyl alcohol. After a second inspection under the microscope the point was allowed to oxidize for several days in a dry oxygen atmosphere. The flat superconductor (post) was prepared in a similar fashion.

We found an optimum point to be one having a radius of curvature of 5-15 microns and being free from burrs and sharp edges. For the most part, sharper points produced junctions that were predominately weak link character, often showing considerable hysteresis in their current voltage characteristics and very low responsibities to far infrared radiation. With careful adjustment, these sharp points often produce high resistance junctions (that is, with shunt resistances $> 100\Omega$). Usually

such junctions showed very small critical currents rounded by thermal noise, and little or no measurable ac Josephson effect. Overly blunt points, on the other hand, displayed excellent ac Josephson effects but had low shunt resistances and small differential resistances near V=0.

Points whose tips were deformed during a run or whose oxide layer had been too abraided were warmed to room temperature and resharpened. Usually only the No. 400 emery paper needed to be used. Then they were set aside and allowed to re-oxidize.

4. Sample Adjustment

Typically, the cryostat was cooled to liquid He temperatures with the point contacts separated. The points were brought into contact while monitoring the current-voltage characteristic. We found that during a single run several different junctions could be formed. While decreasing the separation of the yoke arms, we could routinely generate junctions whose current-voltage characteristics went from wholly resistive, to partly weak link-partly Josephson, to completely weak link. The most radiation sensitive junctions were those showing a considerable ac Josephson effect, as described above. Generally we require a continuous, high, differential resistance near zero voltage, although occasionally we used a 5 ohm junction shunt to bias along an unstable region connecting the critical current to the resistive portion of the characteristic. We found junctions withacceptable radiation sensitivies having shunt resistances varying from 1 to 10^3 ohms. Typically we used a junction with the largest shunt resistance which showed sufficient ac Josephson effect to be radiation sensitive.

C. Resonators

We have constructed several types of junction-resonator systems, shown in Fig. 7. The superconductors enter the resonator through

epoxy-insulated holes in the walls, and the far infrared power is fed in via the focusing cones at the top of each resonator. The resonators were machined from brass in separate sections and press fit together. In order to increase resonator Q's we also fabricated single piece resonators by electroforming copper onto an aluminum mandrel, although we observed no measurable increase in Q's.

The purpose of the focusing cones was to reduce the cross-sectional area of the far infrared beam in order to minimize the resonator losses at the coupling hole. With f/1.5 radiation in a 1.1 cm i.d. light pipe, the minimum cone exit diameter allowing all the radiation through is about 3.5 mm. This was the coupling hole diameter used in Fig. 7, A. B, and D. In the geometry shown in Fig. 7C, the cone exit diameter was 1.5 with the radiation being propagated into the resonator in a coaxial mode.

D. Electrical Measurements

In Fig. 8 we show the biasing circuit used to measure to the dc properties of the point contact. Essentially it shows a programmable current source and both dc and ac voltage pickup networks. With it we routinely measure (i) the dc current (ii) the differential resistance (= dV/dI), and (iii) the junction response to radiation as a function of the junction voltage. Additionally, the fixed current mode is used to bias the junction for the spectral response measurements. The dc power supply is a pair of 10.7 volt mercury batteries connected across a 5KΩ helipot. The "T" filter reduces the contact noise generated when sweeping the helipot. The current measuring resistors (R_I) were available in decade steps from 1 to $10^6\Omega$ while a junction shunting resistor (R_S) of 1 or 10 ohms was available to reduce the bias circuit impedance.

When initially adjusting the point contact's characteristic, an audio frequency signal generator is connected to the AC_{in} terminals. The current-voltage characteristic is monitored by dc coupling the I and V terminals to a pair of Tektronix 1A7 plug-in preamps in a Type 536 oscilloscope chassis. The transformer T1 provides isolation from the single ended signal generator and C1 is a dc blocking capacitor.

Having found an adequate junction, its characteristics are recorded using a motor drive on the helipot. The current and voltage terminals are connected to the X and Y axes of a X-Y recorder and the voltage measured as a function of bias current. The dV/dI and response data are measured by passing the ac junction voltage through T2 to a narrowband amplifier and coherent detector. To measure dV/dI, a small amplitude audio frequency signal is connected to AC_{in} and the resultant amplified audio frequency junction voltage is recorded versus dc voltage. To measure the junction far infrared response, the ac voltage source is removed from AC_{in} and chopped radiation from the interferometer is applied to the junction. The amplified junction signal is then recorded as either the current bias or the interferometer path differerence is swept.

The purpose of T2 (a Triad G-10 geoformer) is two-fold: (i) it provides electrical isolation between the junction circuitry and the single ended input of the narrow band preamp, and (ii) it also provides noise free gain with common mode rejection. Since the differential resistance of most junctions is on the order of several ohms, a transformer with a voltage gain of 10^2 may be usefully employed to match the junction resistance to the 1MΩ preamp input impedance. The transformer has balanced windings on both primary and secondary and can be wired to provide about 40 db of common mode rejection. It is wired so that it can be used to provide

voltage gains of 20, 40, 100 and 300, the first three with common mode rejection. With the ×100 transformer the coherent detector measures a noise voltage of 3×10^{-9} volts in a 1Hz bandwidth. (Johnson noise in a 100Ω resistor at 300°K is about $2\mu V/\sqrt{Hz}$.) Two Sanborn 8875A differential amplifiers were available for amplification of low level dc current and voltage signals.

The electrical measurements on the junction are made using a conventional four terminal network with the two current leads of No. 36 copper wire and voltage leads of No. 40 manganin. Cables connecting the bias box to the cryostat are shielded with braided ungrounded guards and the whole cable enclosed in a flexible Mu-metal shield.

This shielding reduces the 60 Hz inductive pickup to a level below the white noise seen by the coherent detector. Equally important, the junction is surrounded by a can tinned with tin-lead solder to screen 60 Hz magnetic fields, and the entire lower portion of the cryostat surrounded by two concentric Mu-metal shields, which reduced the laboratory magnetic field by a factor of 100.

E. Cryogenics

All of the experiments we carried out in a conventional glass dewar 5 cm i.d. and 90 cm long surrounded by a liquid nitrogen bath. With an initial one liter charge of liquid helium, junction temperatures below 5°K could be maintained for up to 18 hours. Included in the dewar assembly was a two-inch pumping line allowing for measurements to be made down to 1.2°K. Absolute temperature measurements were made using an aneroid barometer to measure the helium vapor pressure.

We regulated the temperature of the pumped helium using a throttled pumping line valve for grass control and a thermometer bridge[40] for fine

control. The bridge used a 67Ω Allen-Bradley carbon resistor as a thermometer and a 200Ω manganin coil as a heater. Temperatures above the λ-point could be easily controlled to a few millikelvin.

V. RESONANT DETECTION

In Sec. II, we showed that a Josephson junction coupled to a resonant cavity can emit radiation. In this section we will show that the junction's self detection of the emitted radiation can be very sensitive to externally applied radiation at the Josephson frequency. We will use this property to construct a high-sensitivity, narrowband, far infrared detector.

We shall employ a model introduced by Werthamer[29] and Werthamer and Shapiro (WS)[41] to describe the behavior of a Josephson junction whose ac current is coupled to a high Q resonant cavity. We begin by calculating the current in a voltage-biased junction, given by

$$I(t) = \cos \{\omega_0 t + \int^t \Omega(t')\, dt'\} \tag{21}$$

where $I(t)$ is the Josephson current in units of the maximum Josephson current, I_1, $\omega_0 = 2eV_{dc}/\hbar$, and $\Omega(t) = 2eV_{ac}/\hbar$. For convenience we have let the dc phase $\Phi_0 = \pi/2$ without loss of generality.

The model is based on the following ideas: (i) the ac Josephson current at frequency ω_0 radiates electromagnetic energy which can be stored in a resonator mode; (ii) the resonator electric field determines the rf voltage across the junction; and (iii) the rf voltage across the junction determines the amplitude of the ac currents at ω_0. We will contruct equations representing the coupled junction resonator system and solve self consistently for the ac voltages.

We will first discuss this basic model due to Werthamer and Shapiro and then consider the effects of a second term driving the resonator, an externally applied rf voltage. We shall show that, under certain conditions, the junction resonator system is an excellent detector of applied ac voltages, i.e. when $\omega_{rf} = \omega_0 = \omega_c$ (the resonator frequency) and when the

junction-resonator coupling is strong.

A. Undriven Self-Induced Step

Consider Maxwell's equation in free space ($\mu = \epsilon = 1$):

$$\vec{\nabla} \times \vec{E} = 1/c \, \overset{\circ}{\vec{H}}$$

$$\vec{\nabla} \times \vec{H} = 4\pi/c \, \vec{j} + 1/c \, \overset{\circ}{\vec{E}}$$

or

$$\nabla^2 \vec{E} - 1/c^2 \, \overset{\circ}{\vec{E}} = 4\pi/c^2 \, \overset{\circ}{\vec{j}} \tag{22}$$

Assume that the current drive for this wave equation is a point contact Josephson junction, so that $\vec{j}(\vec{x},t)$ may be represented as a point current source. Now except at the current sources, (22) reduces to $\nabla^2 \vec{E} - \overset{\infty}{\vec{E}}/c^2 = 0$ which can be solved according to the boundary conditions imposed by the metallic surfaces of the resonator and the superconductors forming the junction. Given such solutions, at any point in the resonator, $\nabla^2 \vec{E} = -\omega^2/c^2 \vec{E}$, at the current source we can approximate (22) by

$$\left[\frac{d^2}{dt^2} + \omega_c^{\,2} \right] \vec{E} = -4\pi \frac{d\vec{j}}{dt} \tag{23}$$

Adding a phenomenological damping term to the wave equation to account for losses in the resonator, (23) becomes

$$\left[\frac{d^2}{dt^2} + \gamma \frac{d}{dt} + \omega_c^{\,2} \right] \vec{E} = -4\pi \frac{d\vec{j}}{dt} \tag{24}$$

where $\gamma = \omega_c/Q$ and Q is the quality factor of the resonant mode. Throughout this discussion we will restrict our attention to a single mode of the system, although in general several modes may be driven simultaneously. For the physical parameters of interest only a single mode will play an important role.

Now integrating (24) with respect to time and spatially across the junction insulator, and substituting (21) for the driving current we find

$$\left[\frac{d^2}{dt^2} + \gamma \frac{d}{dt} + \omega_c^{\,2}\right] \int^t \Omega(t')\, dt' = +A \cos\left[\omega_0 t + \int^t \Omega(t')\, dt'\right] \qquad (25)$$

where $A = -j_1 \frac{2eI_{-1}}{\hbar C}$, which will be treated as an empirical quantity determined by the geometric cooling of the junction current to the resonator. Werthamer and Shapiro[37] have solved (25) on an analog computer and have found that for moderately high Q resonators ($Q \sim 10$), and for $\omega_0 \sim \omega_c$, the rf voltage in the resonator is essentially monochromatic, with frequency ω_0. They also obtained analytic solutions by making the approximation that

$$\int^t \Omega(t')\, dt = \xi \sin(\omega_0 t + \phi) \qquad (26)$$

where ξ, ϕ are real quantities which are to be found by solving (25) at the frequency ω_0. For large enough Q, the harmonics of ω_0 in the driving current will not induce appreciable rf voltage components in the resonator and can be neglected.

Let us first calculate the current in the junction at the frequency ω_0: $I(t) = \cos[\omega_0 t + \xi \sin(\omega_0 t + \phi)]$ or using the Fourier decomposition

$$I(t) = \sum_n J_n(\xi) \cos[(1+n)\, \omega_0 t + n\phi] \qquad (27)$$

The components at ω_0 are

$$I_{\omega_0}(t) = J_0(\xi) \cos(\omega_0 t) + J_2(\xi) \cos(\omega_0 t + 2\phi), \qquad (28)$$

where we have used $J_{-n}(\xi) = (-1)^n J_n(\xi)$. This expression can be rearranged into a more tractable form

$$I_{\omega_0}(t) = \mathcal{D}_1(\xi, \chi) \cos(\omega_0 t + \phi + \xi) \qquad (29)$$

where

$$\mathcal{Q}_1(\xi,\chi) = \frac{2J_1(\xi)\ J_1'(\xi)\ \sec\chi}{[\xi^2\ J_1^{\ 2}(\xi) + J_1^{\ 2}(\xi)\ \tan^2\chi]^{1/2}} \tag{30}$$

and

$$\tan\chi = -\frac{\xi J_1'(\xi)}{J_1(\xi)}\ \tan\phi \tag{31}$$

where we have used $J_{n-1}(\xi) + J_{n+1}(\xi) = \frac{2n}{\xi} J_n(\xi)$ and also $J_{n-1}(\xi) - J_{n+1}(\xi) = 2\frac{d}{d\xi} J_n(\xi) \equiv 2J_n'(\xi)$.

Now the rf current given by (29) drives the rf voltage in the cavity while the rf current necessary to produce $\xi\ \sin(\omega_0 t + \phi)$ is given by $[d^2/dt^2 + \gamma d/dt + \omega_c^{\ 2}]\ \xi\ \sin(\omega_0 t + \phi)$. Equating this to (29) gives the self consistent equations for ξ and ϕ. After some manipulation we find:

$$\xi\cos\ (\omega_0 t + \phi + \theta) = \Gamma\ \cos\theta\,\mathcal{Q}_1\ (\xi,\chi)\ \cos\ (\omega_0 t + \phi + \chi) \tag{32}$$

where

$$\tan\theta = \frac{\omega_0^{\ 2} - \omega_c^{\ 2}}{\gamma\ \omega} \tag{33}$$

$$\Gamma = A/\gamma\omega \quad . \tag{34}$$

Physically θ is the phase angle between the driver of the damped harmonic oscillator (the rf current) and the driven (the rf voltage) and Γ is the dimensionless coupling constant of the junction current to the resonator mode.

Since (32) is valid independent of time, its amplitudes and phases must be equal. Phase equality implies that $\tan\theta = \tan\chi$, and amplitude equality implies that $\xi = \Gamma\ \cos\theta\,\mathcal{Q}_1(\xi,\chi)$. Combining these gives an implicit equation for ξ and an explicit one for ϕ:

$$\xi/\Gamma = \frac{2J_1(\xi)\ J_1'(\xi)}{[\xi^2 J_1'^2(\xi) + J_1^{\ 2}(\xi)\ \tan^2\theta]^{1/2}} \tag{35}$$

and

$$\tan \phi = - \frac{J_1(\xi)}{\xi J_1'(\xi)} \tan \theta \tag{36}$$

We have solved (35) graphically in Fig. 9. Both sides of the equation are plotted against ξ. The L.H.S. of (35) is plotted for various values of the parameter Γ, while the R.H.S. is plotted for various θ. The intersection of the curves gives the operating point of the junction-resonator system for specified Γ (the coupling) and $\tan \theta$(the Josephson frequency relative to the resonator frequency). References 29 and 41 gives extensive discussions of the solutions and associated dc currents which are calculated from (21). These have the form $I_{dc} = J_1(\xi) \cos \phi$ and can be shown to be equal to $\xi^2/2\Gamma$, where ξ satisfies (35).

Note that the R.H.S. of (35) is just the amplitude of the ac Josephson current at ω_0 in phase with the rf voltage ξ. Its functional dependence on ξ is derived wholly from Josephson's equations for the ac currents. As the phase angle θ, increases from zero, the in-phase current decreases. As ξ increases, the current amplitude also increases as non-linearities in the junction draw power from the fundamental (power in the sense that the ac current power $\mathcal{I}_\omega^2$ obeys a conservation law derivable from $\sum_n J_n^2(\xi) = 1$.) At $\xi = 1.841$, corresponding to $J_1'(\xi) = 0$, the rf voltage saturates. Any ξ larger than 1.841 drives the rf current negative, shifting the junction-resonator system to an unphysical operating point. As Γ increases the rf voltage remains at 1.841 while the rf current decreases, reflecting the more efficient coupling.

In Appendix C we discuss the first order corrections to our assumptions that the rf voltage is monochromatic. We show that the amplitude of the nth harmonic is proportional to $\Gamma/[n^2 + Q^2(n^2-1)^2]^{1/2} \simeq \Gamma/Qn^2$. For Q=10, the 2nd harmonic contributes about 2% to the total ac voltage in the resonator. The main effect of non-zero harmonic voltages on the operating

point of the system is to slightly round the saturation point of ξ indicated by the sharp knee in Fig. 12. Generally, the small amplitudes of the harmonic voltages indicates that the WS model is much more accurate than one might initially have expected.

This model should accurately predict the amplitude of the radiated power from the junction. Since the Josephson current equation conserves energy, the dc power into the junction ($= I_{dc}\,\hbar\omega_0/2e$) is the rf power radiated by the junction. Since the reported detected powers of Josephson radiation from point contacts are orders of magnitude less than the dc input power, the conductance shunting the point contact may play an important role. The phenomenological damping constant, γ, introduced in (24) to give the resonance a finite Q can be related to an effective junction shunt conductance, G_{eff} by $G_{eff} = \gamma C$, where C = junction capacitance. Using (34) we find

$$G_{eff} = 2eI_1/\hbar\omega_c\Gamma \tag{37}$$

According to the WS theory, the dc power input goes into rf ohmic losses in this effective conductance. There are two contributions to G_{eff}: the losses in the resonator (losses in the cavity walls and out the coupling hole) and loss in the conductance shunting the junction. Using typical experimental numbers in (37) indicates that G_{eff} may be dominated by the observed junction shunt conductance. For example, using $G_{eff} = G = 0.1\Omega^{-1}$ as taken from a typical point contact's I-V characteristic, $I_1 = 100\mu A$, $\omega_c = 10^{12}$ cps, we find from (37) that $\Gamma \sim 4$. Observable self-induced steps are generated for $\Gamma \sim 0.5$-5. Even in a lossless resonator ($Q = \infty$) we require that $I_1/G > 0.5$ mV to saturate the rf voltage.

We should point out that junction resonator system will emit radiation whenever $m\omega_0 \sim \omega_c$; i.e., some harmonic of the Josephson frequency may drive the resonant mode. The calculation of rf voltage amplitudes proceeds parallel to what we have presented. The rf voltage saturates for large Γ on ξ such that $J_n'(\xi) = 0$, although the equations require a minimum

Γ for oscillation. The frequency of the emitted radiation is at $m\omega_0$. Whether the system is oscillating at the fundamental Josephson frequency or some harmonic of it, can be determined by measuring the ratio of the Josephson frequency to the frequency of the emitted radiation, or perhaps more easily via the junction resonator's detection properties as discussed below.

B. Driven Self Induced Step

The effect of externally generated rf voltages on the operating point of the junction resonator system may be divided into two classes: non-resonant detection - when $\omega_{rf} \neq \omega_0$, and resonant detection - when $\omega_{rf} = \omega_0$. This difference between the two will be shown to be essentially between broad and narrow band detection. We will consider each in turn.

1. Non-resonant Detection

WS showed that adding a externally generated microwave voltage to the junction resonator system results in mixing of the harmonics of the microwave frequency with the Josephson frequency, allowing the junction to oscillate whenever $\omega_0 + p\omega_{rf} \sim \omega_c$. Specifically WS assumed that the effect of the microwaves is to induce across the junction an additional voltage of $(\hbar\omega_{rf}\ \xi_{rf}/2e)\cos\ \omega_{rf}t$. Then (25) with (26) becomes

$$\left[\frac{d^2}{dt^2} + \gamma\frac{d}{dt} + \omega_c^2\right]\xi\sin(\omega_0 t + \phi) \tag{38}$$

$$= A\cos\left[\omega_0 t + \xi\sin(\omega_0 t + \phi) + \xi_{rf}\sin\omega_{rf}t\right]$$

$$= A\sum_p J_p(\xi_{rf})\cos\left[(\omega_0 + p\omega_{rf})t + \xi\sin(\omega_0 t + \phi)\right]$$

In this case, the problem is equivalent to the undriven oscillator if we let $\omega_0 + p\omega_{rf} \sim \omega_c$ and replace Γ by $\Gamma J_p(\xi_{rf})$ in (35). The resultant dc current turns out to be the same as before i.e., $I_{dc} = \xi^2/2\Gamma$. Now the system can oscillate whenever $\omega_0 \sim \omega_c - p\omega_{rf}$. For $\xi_{rf} \ll 1$, as is the case

for available power from the far infrared interferometer, only the fundamental (p=0) self induced step is affected. The change in dc current due to the far infrared radiation is $\Delta I_{dc} = \frac{1}{2\Gamma} \Delta(\xi^2)$. The change in ξ^2 is due to the change in $\Gamma J_0(\xi_{rf})$ used to solve for ξ in (35), so $\Delta I_{dc} = \xi/\Gamma \quad \Delta\xi = \xi/\Gamma\,(d\xi/d\Gamma)\,\Delta\Gamma$. But $\Delta\Gamma = \Gamma\Delta(J_0(\xi_{rf})) \cong \Gamma\,\xi_{rf}^2/4$ so

$$\Delta I_{dc} = -\,\xi \quad d\xi/d\Gamma \quad (\xi_{rf}^2/4) \tag{39}$$

Since ξ_{rf}^2 is proportional to the applied microwave power, the detection (i.e. the change in I_{dc}), is linear in the applied power. The sensitivity, $d\xi/d\Gamma$, can be calculated from (35) or from Fig. 12. It varies from unity when ξ=0 to zero when ξ saturates.

Note that the response of the self induced step is essentially broadband- that is; it does not directly depend on ω_c. However, as we show below, coupling the applied rf voltage to the junction depends strongly on the properties of the resonance.

2. Resonant Detection

The above analysis must be redone when the frequency of the applied radiation is the same as the oscillation frequency. Then the applied rf voltage and the junction generated voltage must be treated equivalently. In addition, we will introduce the applied rf voltage into the problem is a more physical fashion.

In the previous section we assumed that the applied rf voltage couples directly to the junction, giving a junction response that is independent of frequency. A more reasonable assumption is that it couples to the resonator and is detected by the junction as the junction detects the total rf voltage in the resonator. In that case (25) becomes

$$\left[\frac{d^2}{dt^2} + \gamma \frac{d}{dt} + \omega_c^2\right] \int^t \Omega(t')dt' = A \cos\left[\omega_0 t + \int^t \Omega(t')dt'\right] + B \frac{d}{dt} V_{ext}(t), \tag{40}$$

where B is some constant representing the coupling of the applied rf voltage to the resonator, and $V_{ext}(t)$ is the applied voltage. If $\frac{d}{dt} V_{ext} = \xi_{rf} \cos(\omega_{rf} t + \phi_e)$, then the appropriate rf junction voltage is

$$\int^t \Omega(t')dt' = \xi \sin(\omega_0 t + \phi) + \xi_1 \sin(\omega_{rf} t + \phi_1) \tag{41}$$

If ω_0 and ω_{rf} are unequal, this procedure turns out to be equivalent to that discussed previously with $\xi_1 = \xi_{rf} \cos\theta_{rf}$, where $\tan\theta_{rf} = (\omega_{rf}^2 - \omega_c^2)/\gamma\omega_{rf}$. That is the amplitude of the applied voltage on the junction is determined by the natural line width of the resonator.

When the frequency of the applied radiation is equal to the Josephson frequency,, then the rf voltage across the junction reverts to the form given in (26). Putting this in (40) and letting $\omega_{rf} = \omega_0$ we get

$$\xi \cos(\omega_0 t + \phi + \theta) = \Gamma \cos\theta\, \mathcal{Q}_1(\xi, X) \cos(\omega_0 t + \phi + X) + \Gamma_e \cos\theta\, \xi_{rf} \cos(\omega t + \phi_e). \tag{42}$$

Γ_e is now some dimensionless coupling of the radiation into the resonator, and Γ, θ, and $\mathcal{Q}_1$ are given in (30-34). As before ξ is the total rf voltage in the resonator, but here it is driven by two sources: (i) the rf Josephson currents of amplitude $\mathcal{Q}_1(\xi, X)$ coupled to the resonance through Γ; and (ii) the applied rf voltage (signal) coupled through Γ_e. Rearranging (42) and letting $x = \Gamma_e Z_{rf}$, we have

$$\Gamma \cos\theta\, \mathcal{Q}_1 \cos(\omega_0 t + \phi + X) = F \cos(\omega t + \phi + \psi) \tag{43}$$

where

$$F = [\xi^2 + 2\xi x \cos\theta \cos(\phi + \theta - \phi_e) + x^2 \cos^2\theta]^{1/2} \tag{44}$$

$$\tan \psi = \frac{\xi \tan \theta + x \sin (\phi_e - \phi)}{\xi + x \cos (\phi_e - \phi)} \tag{45}$$

We can equate the phases and amplitudes of (43) to get

$$F = \Gamma \cos \theta \, \mathcal{L}_1 (\xi, X) \tag{46}$$

$$\tan X = \tan \psi \tag{47}$$

Using (30) and (31) we can show that the implicit equations (46) and (47) reduce to

$$(2\Gamma J_1 J_1')^2 = [\xi J_1' (\xi + x \cos(\phi - \phi)]^2 + [J_1 (\xi \tan \theta + x \sin (\phi - \phi)]^2 \tag{48}$$

and

$$\cos \phi = \frac{\xi}{2\Gamma J_1} [\xi + x \cos (\phi_e - \phi)] \tag{49}$$

the dc current is $I_{dc} = J_1 \cos \phi$ which becomes

$$I_{dc} = \xi/2\Gamma [\xi + x \cos (\phi_c - \phi)] \tag{50}$$

where $J_n = J_n(\xi)$. These three equations (48-50) contain the solution to the problem. The response of the self-induced step is given by (50) where ξ depends on x and ϕ explicitly in (48), and ϕ depends on x implicitly in (49). Our method of deriving these equations involved looking at the problem backwards. We considered the Josephson current at ω_0 as driving two rf voltages (the resonator voltage and the "applied" voltage), only one of which couples back onto the junction.

To arrive at a meaningful expression for the system's response to the far infrared signal ($\propto x^2$), we expand (50) in a Taylor series to second order in x^2 around $x=0$ [where ξ, ϕ are given by the imperturbed solution]. We then use (48,49) to evaluate terms such as $d\xi/dx$, $d^2\xi/dx$, $d/dx \cos (\phi_e - \phi)$ and their products. Also, keeping in mind that the applied

voltage is in fact due to broadband, incoherent radiation, we will average over ϕ_e, the phase of applied voltage. That is, the dc current is observed over a time period on the order of seconds. The phase ϕ_e will remain constant over this time period only for radiation in a bandwidth of ~1Hz. The power (or number of photons) in this bandwidth is negligible in our experiment.

The results of this calculation have been evaluated numerically and are plotted in Fig. 10. We show the response linewidth versus $\tan\theta = (\omega_0^2 = \omega_c^2)/\gamma\omega$ $[\approx (\omega_0-\omega_c)/\omega_{1/2}$ for $\gamma/\omega \ll 1$, where $\omega_{1/2}$ is the half width point]. For $\Gamma=0$ we see the natural line width of the resonator, unaffected by the junction-resonator feedback. As $\Gamma \to 2.91$, the response becomes singular, corresponding to ξ saturating on 1.841. We also note that in contrast to the zero voltage response, the self induced step increases when rf voltage is applied to the system. A similar singular response is obtained for the problem as formulated in Section V.B1 (where applied radiation couples directly to the junction). Due to the different form of the equations relating rf voltages to observed dc currents, the response of the self induced step height is such that the applied rf voltage decreases the step height.

The response singularity can be given a simple physical interpretation based on the behavior of ξ vs $\mathcal{J}_1(\xi)$ in the unperturbed problem when $\omega_0=\omega_c$. The dc current can be shown to be $1/2\mathcal{J}_1(\xi)\xi$ for all Γ. When $\Gamma > 2.91$ the rf resonator voltage, ξ, is saturated at $\xi = 1.841$. The junction is unable to drive the resonator at any higher level as Γ is increased. If, when we are in this saturated region, we apply additional rf voltage, the amplitude of the rf resonator voltage increases. But we are operating in a region where $\partial\mathcal{J}_1/\partial\xi$ is infinite so any change in ξ implies an infinite

change in $\mathcal{J}_1(\xi)$ and so also in the dc current. In fact, a careful analysis shows that the response diverges as $(d\mathcal{J}_1/d\xi)^3$. In addition the applied rf voltage shifts the effective value of tan θ slightly. As $\Gamma \to 2.91$ the right hand graph in Fig. 9 shows that ξ also changes markedly, contributing to the singular response.

This predicted singular response is believed to be a fundamental feature of the coupled junction resonator system. It can be shown that the presence of harmonics of the Josephson frequency shifts the system's operating point only slightly, leaving intact the sharp saturation of ξ at 1.841. Quantitative estimates of the contribution of harmonics to the response are difficult to make due to the complexity of the form of such contributions.

We can also develop the same sort of theory as we have done here for the case where $m\omega_0 \sim \omega_c$. The results are similar in that the response is singular when Γ is such that $J_m'(\xi) = 0$. The major difference is that the singular response is now at $m\omega_0$, so that the peak response is now at some subharmonic of the Josephson frequency. This should provide the simplest test on which harmonic of the Josephson frequency the junction-resonator system is oscillating.

C. Zero Voltage Detection

The effect of the junction-resonator coupling can be calculated from (42) by letting $\omega_0=0$. In that case we obtain

$$\xi \cos(\omega t + \phi + \theta) = 2\Gamma \cos\theta\, J_1(\xi) \sin\phi_0 \sin(\omega t + \phi) + \Gamma_e \xi_{rf} \cos\theta \cos(\omega t + \phi_e) \tag{51}$$

where we have now included the dc phase across the junction. Since the dc current is $J_0(\xi) \cos\phi_0$, and we are measuring its maximum value,

$\cos\ \phi_0 = 1$, $\sin\ \phi_0 = 0$. There are no ac currents in the junction and so no junction-resonator feedback. The only rf voltage is the resonator is that due to the applied voltage. That is, $\xi = \Gamma_e\ \xi_{rf} \cos\theta$, which gives a dc current of $J_0(\Gamma_e \xi_{rf} \cos\ \theta)$, and, in the limit of $\Gamma_e\ \xi_{rf} \ll 1$,

$$\Delta I_{dc} = -\ 1/4\ (\Gamma_e\ \cos\ \theta)^2\ (\xi_{rf})^2 \qquad (52)$$

where $\cos^2\theta = (\gamma\omega_{rf})^2/[(\omega_{rf}{}^2 - \omega_0{}^2)^2 + (\gamma\omega_{rf})^2]^2$ gives the Lorentzian line shape of the assumed resonator response. We can thus use the zero voltage response to measure the natural line width of the resonator. This frequency dependence to the response is believed to dominate the "broad-band" response of the zero voltage critical current discussed in Section II.C. and VI.C.

VI. EXPERIMENTAL RESULTS

A. Resonant Detection

We show in Figs. 11 - 13 typical measurements made on a point contact junction coupled to a resonant cavity. Here the self-induced step occurs at $\pm$ 392 μV, showing up most clearly on the plots of dV/dI. The response of the junction to broadband far infrared radiation is also shown. Figure 12 shows the same junction as Fig. 11 with a slightly different applied magnetic field. Figure 13 shows the spectral response of the junction shown in Fig. 12 when biased at the differential resistance maximum at about 350 μV. The figures show most of the effects that we have discussed above.

The current-voltage characteristic in Fig. 11 shows a continuous transition from the supercurrent step at $\bar{V} = 0$ to the resistive state at $V > 0$. The behavior agrees with the McCumber model[36] discussed in Section III. Note the lack of any contribution due to capacitive loading of the junction. The rounding of the transition between the supercurrent step and resistive state is believed due to thermal noise tending to decouple the phases of the superconductors.

The self-induced step shows a similar rounding. This rounding may be due in part to the finite Q of the resonator. In the last section we showed that the junction current can couple to the resonator for a range of dc voltage biases. That is, for certain values of Γ, the junction will carry appreciable dc currents for $|\omega_o - \omega_c| \lesssim \omega_c/Q$. The total step height is probably due to dc currents from the entire range of dc voltages, since, according to McCumber, the dc current at a given voltage is sensitive to dc currents at nearby voltages. For self-induced steps

due to reasonably high Q resonances, we might represent the current-voltage behavior near $\omega_o = \omega_c$ as being due to the existence of a sharp, well defined step at ω_c with a height proportional to $\int_0^\infty d\omega_o I_{dc}(\omega_o)$. This sharp step is then connected to the resistive portion of the characteristic by large differential resistances similar to those near V=0.

In Fig. 12, showing the same junction in a slightly different magnetic field, the details of the I-V curve are noticeably altered due to the redistribution of Josephson currents within the point contact. Such sensitivity to magnetic fields is easily understood if the point contact is composed of a number of junctions. The change in the zero-voltage supercurrent is the interference effect discussed in Section II. The change in the induced step is probably due to field induced changes in Γ. If several parallel Josephson junction are radiating simultaneously, the applied dc magnetic field controls the relative phase of the radiation from each junction.[42] For example, if there is one-half of a fluxoid in the area between two radiating junctions, the radiation emitted by the two will be 180° out of phase. If the two junctions carry the same rf currents then no radiation is emitted. Since a single point contact junction may have many microscopic contacts, the magnetic field dependence of the junction-resonator coupling is expected to be quite complex. We believe that our failure to observe more often the self-induced steps may be due in part to the sensitivity of the coupling to dc magnetic fields.

The system response to broadband far infrared radiation (shown in the lower curves in Figs. 11 & 12) has two contributions. The response curves are dominated by the junction response to the changes in the zero-voltage critical current. This response dependence on dc bias agree with

that predicted by the McCumber model (lower curve in Fig. 3) with account taken of the thermal rounding.[37] Superimposed on the "broadband" response is the resonant response due to the self-induced step. In agreement with the theory of Sec. V, the self-induced step height increases as the radiation is applied. Measurements of the response spectra show that within each response region the spectra are independent of bias.

Figure 13 shows the resonant response when biased at 250μV. The dominant contribution is due to the resonator mode at 6.34 cm^{-1}. At 3.5cm^{-1} is a contribution from the zero-voltage response. This peak is due to another resonator mode whose self-induced step does not appear in this particular junction. The zero-voltage response also shows the effect of the 6.34 cm^{-1} mode, unnarrowed by the junction-resonator feedback. Its measured linewidth is 0.7cm^{-1}. The resonance-narrowed linewidth is much smaller than the interferometer's resolution of 0.2 cm^{-1}, and the (sin x)/x line shape in Fig. 13 is the interferometer's spectral window. From the interferogram, we can place an upper limit of 0.01 cm^{-1} on the line width. Even at 50mm path difference, the response shows no observable damping associated with a non-zero line width.

We note that the 6.34 cm^{-1} response corresponds via the Josephson relation to 392 μV. That is, the response peak corresponds to the measured self-induced step voltage. This correspondence is characteristic of all the observed resonant responses. Figure 14 shows a plot of those resonant responses we could associate with well defined self-induced steps. The solid line is the Josephson relation $2eV=h\nu$. In each case the junction-resonator system is responding to radiation as if $\omega_o = \omega_c$. This indicates that for all observed radiation-sensitive self-induced

steps, the fundamental Josephson frequency is driving the resonator.

We observed the resonant response in all of the resonators shown in Fig. 7. We were unable, however, to reliably repeat any experiment concerned with the resonant response. For example, we observed self-induced steps using configuration C in Fig. 7 on only four junctions out of approximately one hundred examined. In one run we observed the resonant response with the point contact in the conical focusing cone. Here ω_c = 8.50 cm^{-1} (the interferogram shown in Fig. 5), and the zero-voltage spectral response showed sharp peaks at 8.5, 10 and 13 cm^{-1}. Yet on other junctions in the identical configuration, the response was only broadband (similar to that shown in Ref. 4, Fig. 8). Such variability was common.

We believe that the variability of the junction-resonator coupling may in part be due to variability of the junction shunt conductance. In Section V we showed that the losses in the resonator could be related to an effective conductance shunting the point contact and further that the effective shunt conductance is typically the same order of magnitude as that observed shunting the junction - i.e. the point contact's impedance may make a significant contribution to the operating point of the junction-resonator system. The condition for saturation of the rf resonator voltage in an infinite Q resonator ($I_1/G \gtrsim .5$ mV) is in practice just attainable with carefully prepared and handled point contacts.

1. Noise Equivalent Power

The usefulness of the system as a detector of far infrared radiation is measured by the system's "noise-equivalent power" (N.E.P.) - that is, the radiation power incident which will give a signal equal to the detector noise. For the response shown in Fig. 13, the signal to noise

ratio of the raw signal is $160/\sqrt{100/2} \sim 20$. At 6.34 cm^{-1}, the radiation power available from the interferometer is $\sim 10^{-10}$ watts/cm^{-1}. With the junction responding to a frequency band width of 0.01 cm^{-1}, the N.E.P. $\sim 10^{-10} \times 10^{-2}/20 \sim 5 \times 10^{-14}$ watts. The interferogram points were averaged over 7 seconds, so if the noise is random, the N.E.P. in a 1 cycle band width is $\sim 10^{-13}$ watts.

Two considerations must be evaluated to understand this N.E.P. figure. The first is that the noise on the spectral response curve is due primarily to drifts in the bias current while the interferogram was being measured, which add white noise to the computed spectral response. The signal-to-noise ratio taken from the raw data is nearly 10^2. The second consideration is that of coupling the power to the resonator. The resonator used in this experiment required the far infrared signal to be coupled to a coaxial transmission line in order to be transmitted into the junctions. We have made transmission measurements on this system and found that at 6 cm^{-1} only 10 percent of the incident power is coupled into the coaxial line. These two corrections give a net N.E.P. of 5×10^{-15} watts/Hz.*

We have attempted to measure the spectral density of far infrared radiation coupled into cavities of various shapes (such as A and B in Fig.7) using 1×2×5mm indium-doped germanium bolometer. The bolometer, in place of the point contact, samples the power density in the resonator that the point contact samples. We found, however, that the bolometer distorted the resonances badly enough to void any comparison of measured spectral

*The noise in the blackbody radiation from room temperature sources, eg., light pipe and chopper, is on the order of 10^{-16} watts/Hz,[43] for a detector band width $\Delta\nu = 10^{-2} cm^{-1}$.

powers with observed point contact response spectra.

The bolometer, by design, absorbs a high fraction of the radiation that hits it and reflects very little. Whatever resonances are present are damped quite heavily by this very lossy element. Additionally, the field distributions in the resonator are changed so much that they greatly change the coupling parameters involved in getting the power into the cavity. The point contact junction and associated bulk superconductors are, by comparison, low loss devices, and the presence of the junction loads the cavity only slightly (even though the junction impedance may in fact dominate the system losses). Resonator C in Fig. 7 was analysed to the extent that we made transmission measurement on it, attributing structure on the normalized transmission spectra to resonant structure of the modes in the resonator. Only a small fraction of the structure on the transmission spectrum showed up as response peaks on the point contact spectral responses, indicating the very selective coupling between resonator modes excited by the incident far infrared power and the junction. In general we were able to find only limited correlation between the transmission spectra and the point contact spectra.

We also measured the transmission spectrum of the system shown in Fig. 7D using back-to-back focusing cones with a 0.75 mm conductor through one of them to simulate the superconductor. The transmission spectrum showed broad structure on it similar to that observed in the frequency responses reported by GRS. Most of the structure they report is probably due to weak resonances in their geometry which dominates the transmission spectra.

We also note another difficulty. It was almost routine to observe

major peaks on the broadband response which could not be identified with self-induced steps; often these peaks were larger and sharper than those associated with self-induced steps. This difficulty is probably due to the distinction between two types of coupling: the coupling of the infrared power into the junction, represented by Γ_R in (12); and the coupling of the rf Josephson currents to the resonator represented by Γ in (34). These two coupling constants are fundamentally distinct. Γ depends on the electric field distribution on the resonator mode, while Γ_R depends on the geometric overlap of junction and displacement currents.

When discussing the self-induced step calculation, in Sec. V, we should have included the effect of Γ_R in the amplitude of the ac voltage induced across the junction. Its only effect is to scale the magnitude of ξ, i.e. in the R. H. S. of (35a) should be replaced by $\Gamma_R\ \xi$.

2. Detector Noise

The source of noise voltage from the detector is not fully understood. The thermal noise in the finite conductance of the junction is certainly a limiting noise, but typically this is a few nanovolts for high quality, radiation sensitive point contacts. Most junctions showed noise voltages one or two orders of magnitude larger than this level. The obvious contribution is due to the great ease with which the junction switches from one dc operating point to another. A point contact composed of many Josephson junctions and weak links in parallel has a number of almost equivalent arrangements of dc currents, depending on the dc magnetic field. In the point contact itself much of the magnetic field may be due to the current flow through weak links. Given some electrical noise on the junction leads, the current distribution in the junction may be

perturbed, and the junction currents rearrange themselves. We have observed that noise pulses from electrical equipment being turned on have irreversibly altered the current-voltage characteristic of the junction, and we believe that low-level noise may induce reversible changes in the junction characteristic which appear as noise on the signal voltage.

The thermal fluctuations which rounded the I-V characteristic of the point contact (discussed in III) certainly contributed to voltage bias fluctuations. We are unable to calculate the magnitude of such contributions, although they are probably smaller than the voltage bias noise due to thermal noise on the bias current through the high differential resistance at a typical bias point.

Fluctuations in blackbody radiation[43] from the light source are not a significant contribution to signal-to-noise ratios observed in our experiments. One can show that the signal-to-noise ratio in blackbody radiation in the Rayliegh-Jeans limit from a source at temperature T is $\sqrt{P/2RT\Delta f}$, where P is the radiation power and Δf is the integration time of the detected signal. Since for any source of interest $kT \gg h\nu$, noise due to the quantized nature of electromagnetic radiation is important.

B. Multiple Junction Effects

Following a report by Clark,[44] we constructed apparatus for forming an array of point contact junctions. Clark demonstrated that such arrays would generate self-induced steps and that the self-induced steps were influenced by the surroundings of the array. We believe that such steps should show detection properties similar to those of a single point contact coupled to a resonant cavity. We were unable to reproduce Clark's results and obtained few results on detection mechanisms due to our inability

to make junctions of high enough quality.

1. Apparatus

The apparatus is shown in profile in Fig. 15. It consists of a frame for holding a planar array of spheres in a hexogonal structure between two brass electrodes. The array is constrained to two dimensions by 0.625 mm thick crystal quartz plates (Q), and pressed together by the electrodes (B) adjusted by screw (A). A Fabry-Perot type of interferometer (R) provided to test for effects on I-V characteristics and spectral responses due to external resonances. Far infrared radiation is fed into the array from the light pipe at the left. Current and voltage leads are attached to electrodes, which were plated with about 0.01 mm of tin.

The superconductors were formed by evaporating approximately 10^4 Å of tin onto the surfaces of 144 copper-berylium bearings.[45] The tin was evaporated at 10^{-6} mm Hg while the bearings were being agitated to expose all surfaces to the evaporant. The spheres were allowed to oxidize in oxygen for several days, then assembled into the sample holder and cooled to liquid helium temperatures. The current-voltage characteristic of the now superconducting spheres was adjusted to exhibit self-induced steps, and I-V curves were measured.

As stated above, our inability to produce high quality, predominantly Josephson, junction limited our results. Ideally, the 144 spheres, in an 12 by 12 array, will form 814 contacts sphere to sphere and sphere to electrode. However, surfaces of the imperfections in the framing mechanism and irregularities on the spheres made the force pushing the spheres together highly irregular. Some contacts would be essentially open circuits, some weak links, and some superconducting shorts. Since we measured the

current and voltage only across the entire array, the contacts of interest, those forming Josephson junctions were both in series with, and shunted by, a variety of resistances. Because of this, we were unable to measure the voltage bias of the structure we observed of the current voltage characteristics. In addition, our adjustment mechanism, for controlling the force compressing the array, was too gross to allow for careful adjustment of current voltage characteristics.

2. Results

In Fig. 16 we show the best of our current-voltage characteristics. Typical of our data, there is no true resistanceless current at zero voltage. The superconducting junctions appear to be in series with a resistance of about 3.2 Ω. The "constant voltage" current steps are regularly spaced and have minimum differential resistivities of somewhat greater than 3.2 Ω and increasing with step number. The array is sensitive to far infrared radiation at the three regions of high differential resistance on either side of the "zero-voltage" current. All three regions gave essentially the same spectral response - that of a narrow peak at 4.3 cm^{-1} with a total width at half maximum of 0.6 cm^{-1}. The response line width for the highest voltage was about 30% less.

We believe these self-induced steps are caused by the junctions generating and detecting electromagnetic radiation at 4.3 cm^{-1}. This frequency, however, corresponds to a dc voltage of 267 μV, while the steps, if we assume a simple resistance in series with the active junctions, are separated by 110 μV. Probably the effective electrical network is considerably more complicated, composed of junctions impeded in an array of resistance. The next simplest model to make is that of a junction-series

resistor shunted by another resistor. Here, the resistors act as a voltage divider, with only a fraction of the junction voltage appearing across the whole network. This gives a shunt resistance of 7.5 Ω and a series of 5.2 Ω(assuming that the first step is, in fact, at 267 μV). But the resistance at high voltage, about 25 Ω, is incompatible with this. The resonance responsible for the self-induced steps is believed to be due to the cavity formed by the Fabry-Perot reflection and the spheres. The microphonics set up when the reflector was moved destroyed the junction, and so no quantative measurement could be made. The problem of microphonics was typical, and we were unable to solve it completely.

Most of the current-voltage characteristics obtained with these array were considerably more complex than that shown in Fig. 16. Figure 17 shows a more representative example, where we have plotted the differential resistance and response versus voltage of an array at 1.85°K. Note the zero offset on the differential resistance curve. The "zero voltage" resistance is about 8 Ω and the resistance varies over only a factor of two over the range of voltages shown. Except at close inspection, the current voltage trace on the oscilloscope is ohmic. The spectral response of the array was measured at the six points labeled by arrows. The three labeled "A" and the three labeled "B" showed identical responses and are shown in Fig. 18.

Some of the ac behavior of the array can be understood by comparing the spectral response curves to their corresponding portions of the current voltage characteristic. Note first that from Fig. 16 the response curve at "B" is of opposite polarity to that at "A". This is understandable if the "B" portion of the response curve is due to a weak self-induced

step appearing on the I-V curve at a slightly higher voltage - i.e., the resistance minimum at 470 μV. The structure on the broadband response curve just maps out the structure on the differential resistance curve. In this case, the self-induced step is due to radiation at 2.8 cm^{-1} as determined from the spectral response "B" in Fig. 18. The spectral response curve "A" is due to the "zero voltage" current change with applied radiation; that is, the change in the zero voltage current of those junctions responding to the applied radiation. There is only a small peak on "A" in Fig. 18 at 2.8 cm^{-1}, and the curve is dominated by the broad structure from 6-12 cms. The intensity of the spectral response is quite temperature sensitive and the peak at 7 cm^{-1} shifts with temperature like the BCS gap over the limited temperature range where we could measure the spectral response.

We present in Fig. 19 the sort of spectral response not at all understood by us. The array is the same tin-coated bearing 0.8 mm in diameter. This spectral response shown is independent of temperature from 3.6 to 2°K, a range of the energy gap of 3-9 cm^{-1}. The source of this spectral response was an I-V characteristic which was completely ohmic ($R \sim 12\ \Omega$) except for two small, almost constant current, voltage steps, at ± 200μV these steps were the only radiation sensitive part of the characteristics. As the bath temperature was reduced the voltage steps moved out on the I-V characteristic and in character approached switching characteristics. Except for these steps, the I-V characteristic was completely ohmic and independent of temperature. The periodic structure on the high frequency tail is believed to be the channel spectra from the 0.625 mm crystal quartz plate covering the array. The feature worth

noting here is that the energy gap for tin at 3.60°K is near 3 cm^{-1}, so the spectral response continues out to more than ten times the energy of the gap.

C. Broadband Response

Our efforts to measure the broadband response of the points contact Josephson junction met with only limited success. With any sort of metallic geometry focusing the far infrared radiation on the points, the spectral response of the zero voltage supercurrent is dominated by resonant modes enhancing the rf voltage at the junction. If all metallic surfaces are removed, the response of the junction is so weak that the detector signal is undecipherable. What we needed was very sensitive junctions and very long integration times. We are searching for effects on the spectral response of the energy gap. So we require that a) the current-voltage characteristic show a well-defined gap edge at $V_{dc} = 2\Delta$ and that b) the junction maintain it far infrared sensitivity over much of it superconducting temperature range.

Figure 4 shows nearly the ideal characteristic. It has a high differential resistance region just above the zero voltage critical and so should have good infrared sensitivity. It also had a clear gap edge indicating a reasonable well defined gap. We arbitrarily define $V(2\Delta)$, the superconducting energy gap, as that voltage which give minimum differential resistivity, although this definition may mis-estimate the actual value of 2Δ due to the presence of excess currents. In Fig. 4 we find $V(2\Delta)$ to be 1.15 mV, which using the BCS gap equation gives at zero temperature, $V(2\Delta) = 1.37$ mV somewhat larger than that given by other measurements.[19]

We chose tantalum as a sample material because of its ease of

fabricating into point contacts. The point and post were fabricated in the usual fashion and, to avoid handling damage, were immediately assembled into the holder. They were again inspected to assure the existence of an unblunted point and then allowed to oxidize. The points were mounted essentially as shown in Fig. 6. The bottom surface of the focusing cone on the end of the light pipe was beveled to prevent radiation from reflecting from the surface back onto the junction.

Figure 20 shows the spectral response of the tantalum junction, whose characteristic is depicted in Fig. 4, at three temperatures within the temperature range of its sensitivity. [At $T > 3.5°K$, the critical current was too small and the differential resistance too low; below $T < 2.67°K$ the I-V characteristic was discontinuous near $V = 0$.] The broad low frequency peaks are due to a series of resonances not quite resolved in the figure. Higher resolution response measurements show a series of response peaks equally spaced at frequency intervals of 0.63 cm^{-1}, running from 2.4 to 6.3 cm^{-1}. The resonances are probably due to the Fabry-Perot resonator formed by the arms of the aluminum point contact holder.

The negative responses in Fig. 20 are probably due to the effects of the energy gap. In the inset in Fig. 20 we plot the minima in the spectral response against the reduced BCS gap as well as the measured $eV(2\Delta)/\hbar e$, where e = electronic charge, $\hbar$ = Planck's constant and C = velocity of light. The precise mechanism for the negative going response is not clearly understood. It may be any of several mechanisms, none of which are supported by available evidence. (i) The interaction of the radiation with the Josephson currents may cause the rf current amplitude to be such that it increases it zero voltage current. Werthamer's

derivation of the frequency dependence of the ac Josephson effect[29] predict the opposite. (ii) The response of the junction may be due to some higher order response - e.g. part of the response is due to the fourth power of the applied rf voltage. In this case the portion of the spectral response between 6 and 10 cm^{-1} should show the resonance structure present at lower frequencies. (iii) The low frequency response could be due to a series of self-induced steps too small to appear as the current-voltage characteristic. Then, these peaks would be such that they would increase the current through the junction while the negative response is the zero voltage response superimposed in the resonance structure. It is, however, unlikely that such self-induced steps would be strong enough to cause the resonant response discussed in Section V and yet not appear at the current-voltage characteristic.

The spectral response curves for another tantalum point in Fig. 21 in the same geometry show the effect of the energy gap much more clearly. The broad high frequency peak is believed to be due to the Riedel singularity in the ac Josephson current amplitude. The peak response frequency is plotted against the reduced BCS gap in Fig. 22 along the value of 2Δ taken from the current voltage characteristics. Spectral response curves were obtained at temperatures ranging from 4.00°K to 2.05°K, corresponding to a range of energy gaps of from 40% to 93% of the zero temperature gap. The low frequency peaks are believed due to a series of resonances which are pulled out in frequency as the peak frequency of the Josephson current is increased. These peaks do not scale with the energy gap.

APPENDIX A

THE DERIVATION OF JOSEPHSON EFFECT

Consider two bulk superconductors that may interact with each other via an interaction Hamiltoniam whose strength we may vary. When the interaction is zero, the two superconductors are independent and may each be characterised by a wavefunction $\psi^{(i)}$, i = 1,2. For convenience, we pick states with fixed numbers of superconducting pairs; i.e., $\psi^{(1)} = \psi_n^{(1)}$, and $\psi^{(2)} = \psi^{(2)}_{N-2n}$. The total system wavefunction is, then, $\psi_n = \psi_n^{(1)} \psi^{(2)}_{N-2n}$. With no interaction ψ_n is degenerate with a large class of wavefunctions with different n. The interaction removes this degeneracy. For instance let the interaction be the tunneling Hamiltonian of Cohen et al:

$$\mathcal{H}_T = \sum_{k,g} [T_{kg}\, a_k^+ a_{-g} + T_{kg}^+ \, a_g^+ a_k]$$

where $\mathcal{H}_T$ transfers an electron from one superconductor, labeled by k, to the other, labeled by g. This one body interaction, when calculated to second order in T_{kg} allows the possibility of transferring a Cooper pair from one superconductor to the other. That is

$$\Delta \quad (\psi_{n+1} \,|\mathcal{H}_T|\, \psi_n) \equiv - HJ_\perp/4e \qquad \text{A-1}$$

We can calculate the interaction energy by ordinary second order perturbation theory. At zero temperature

$$\Delta E = \sum_{\substack{kg \\ k'g'}} \frac{\langle \psi_{n+1} \,|T_{kg}\, a_k^+ \,|\, I \rangle \langle I | T_{kg'}\, a_{k'}^+ a_{g'} |\, \psi_n \rangle}{E - E_I} \qquad \text{A-2}$$

where the intermediate state I has one quasiparticle in it. We are interested in the part of ΔE which has k = -k' and g = -g; that is a Cooper pair (k, -k) is created in one superconductor and another (g, -g) is destroyed on the other. So in the BCS theory (A-2) becomes

$$\Delta E = -4 \sum_{kg} |T_{kg}|^2 \frac{u_k v_k u_g v_g}{\epsilon_k + \epsilon_g}$$

For convenience we have defined $\Delta E = -\hbar J_1/4e$ where $J_1 > 0$. With the interaction as expressed in A-1 the proper combination of wavefunctions is $\psi_\phi = \sum_n e^{in\phi} \psi_n$. Then, to second order

$$\mathcal{H}_T \psi_\phi = \sum_n e^{in\phi} \mathcal{H}_T \psi_n = -\hbar J_1/4e \sum e^{in\phi} (\psi_{n-1} + \psi_{n+1})$$

$$= -\hbar J_1/2e \, \psi_\phi \cos \phi \qquad \text{A-3}$$

The energy coupling the two superconductors is then $\Delta E = -\hbar J_1/2e \cos \phi$.

We can understand the physical meaning of ϕ by considering the effect of shifting the phase of one of the superconducting wavefunctions. Since the many body wavefunction can be written as a product of pair wavefunctions, the phase shift can be accomplished by shifting the phase of each pair function. If $R_\theta^{(2)}$ rotates the phase of $\psi_{2n}^{(2)}$, where n = number of pairs, then $R_\theta^{(2)} \cdot \psi_{2n}^{(2)} = e^{in\theta} \psi_{2n}^{(2)}$ (one factor of θ for each pair). When $\mathcal{H}_T = 0$, the two superconductors are uncoupled and a relative phase change has no meaning. For $\mathcal{H}_T \neq 0$, the phase change has measurable consequences. For

$$R_\theta^{(2)} \psi_\phi = \sum_n e^{in\phi} R_\theta^{(2)} \psi_{n-2n}^{(1)} \psi_{2n}^{(2)}$$

$$= \sum e^{in(\phi+\theta)} \psi_n$$

$$= \psi_{\phi+\theta}$$

So ϕ is the phase difference between the two bulk superconductors. From the arguments in Section II, if the two have different chemical potentials, then $d\phi/dt = 2\Delta\mu/\hbar$, where $\Delta\mu$ is the chemical potential difference.

Since we have defined the original basis wavefunction in terms of well defined numbers of pairs, calculating the current flow between superconductors is a simple matter: let $\hat{n}^{(2)}$ be the number operator

projecting out the number of pairs in superconductor 2. Then $\hat{n}^{(2)}\psi_n = \hat{n}^{(2)}\psi_{N-2n}{}^{(1)}\psi_{2n}{}^{(1)} = n\psi_n$, and the operator $d\hat{n}^{(2)}/dt$ is defined by

$$\frac{d\hat{n}^{(2)}}{dt} = i/\hbar \; [\mathcal{H}_T, \hat{n}^{(2)}]$$

Now

$$\begin{aligned}
\mathcal{H}_T\hat{n}^{(2)}\psi_\phi &= \mathcal{H}_T \sum_n e^{in\phi}\, \hat{n}^{(2)}\, \psi_{N-2n}{}^{(1)}\psi_{2n}{}^{(2)} \\
&= \mathcal{H}_T \sum_n n\, e^{in\phi}\, \psi_N \\
&= -\hbar J/4e \sum_n n e^{in\phi}\, (\psi_{n+1} + \psi_{n-1})
\end{aligned}$$

and

$$\begin{aligned}
\hat{n}^{(2)}\, \mathcal{H}_T\, \psi_\phi &= -\hbar J_1/4e\; \hat{n}^{(2)} \sum_n e^{in\phi}\; [\psi_{n+1} + \psi_{n-1}] \\
&= -\hbar J_1/4e \sum_n e^{in\phi}\, [(n+1)\, \psi_{n+1} + (n-1)\, \psi_{n-1}]
\end{aligned}$$

So

$$\begin{aligned}
[\mathcal{H}_T, n^{(2)}]\psi_\phi &= +\hbar J_1/4e \sum_n e^{in\phi}\, [\psi_{n+1} - \psi_{n-1}] \\
&= -i\hbar J_1/2e \;\; \sin\phi\, \psi_\phi
\end{aligned}$$

Now the net current flow is $I = 2e\, \langle dn^{(2)}/dt \rangle$, so

$$\begin{aligned}
I &= 2e\; i/\hbar \;\; \langle\, [\mathcal{H}_T\; n^{(2)}] \rangle \\
&= J_1 \sin\phi.
\end{aligned}$$

APPENDIX B

ENERGY CONSERVATION IN THE AC JOSEPHSON EFFECT

Consider a Josephson junction with both a dc voltage, $\hbar\omega_0/2e$ and an ac voltage $\hbar\omega_{rf}\xi_{rf}/2e \cos(\omega_{rf}t + \phi_{rf})$ across it. As in Section III the currents through the junction are given by

$$I(t) = I_1 \sum_n J_n(\xi_{rf}) \cos[(\omega_0 - n\omega_{rf})t + \phi_0 + n\phi_{rf}].$$

The junction draws power from the bias circuit when it carries a dc current; i.e., when $\omega_0 = N\omega_{rf}$. At such an operating point, the bias circuit is delivering a power to the junction given by $I_{dc}\, V_{dc}$, where

$$I_{dc} = I_1 (-1)^N J_N(Z_{rf}) \cos(\phi_0 - N\phi_{rf}) \qquad \text{B-1}$$

This power is emitted from the junction as radiation. That is, the junction carries an rf current against an rf voltage. We will calculate this rf power in our simple model of a voltage biased junction and show it to be equal to the dc power input.

We began this discussion with the assumption that the only ac voltage across the junction was at a frequency ω_{rf}. Thus any power radiated by the junction must be at the same frequency. With $\omega_0 = N\omega_{rf}$, the rf current at a frequency ω_{rf} is

$$I(\omega_{rf}) = I_1 \quad J_{-N+1}(\xi_{rf}) \cos[\omega_{rf}t + \phi_0 + (1-N)\phi_{rf}]$$

$$+ J_{-N-1}(\xi_{rf}) \cos[\omega_{rf}t - \phi_0 + (N+1)\phi_{rf}]$$

Letting $\phi \equiv \phi_0 - N\phi_{rf}$ and using some trigonometry identities and Bessel function symmetry relations, the rf current can be expressed by

$$I(\omega_{rf}) = (-1)^{N+1} I_1 \quad J_{N-1}(\xi_{rf}) \cos(\omega_{rf}t + \phi_{rf} + \phi) +$$

$$J_{N+1}(\xi_{rf}) \cos(\omega_{rf}t + \phi_{rf} - \phi)$$

or $I(\omega_{rf}) = I_{rf} \cos(\omega_{rf} t + \phi_{rf} + \theta)$

where

$$I_{rf} = (-1)^{N+1} \; 2I_1/\xi_{rf} \, [\xi^2 J_N'^2 (\xi_{rf}) \cos^2 \phi + N^2 J_N^2 (\xi_{rf} \sin^2 \phi]^{1/2}$$

and

$$\tan \theta = \frac{N J_N}{\xi_{rf} J_N^1} \tan \phi$$

J_N has the argument ξ_{rf} and $J_N' = d(J_N(\xi_{rf}))/d\xi_{rf}$. The rf voltage across the junction is $V_{rf} \cos(\omega_{rf} t + \phi_{rf})$ and so the in phase component of the ac current is $\mathcal{Q}_1 \cos \theta$ and the rf power is

$$P_{rf} = 1/2 \; I_{rf} V_{rf} \cos \theta$$
$$= 1/2 \; (-1)^{N+1} I_1 \frac{2NV_{rf}}{\xi_{rf}} \cos \phi.$$

But $V_{rf} = \hbar\omega_{rf} \xi_{rf}/2e$ and using (B-1) we have

$$P_{rf} = - \frac{N\hbar\omega_{rf}}{2e} I_{dc} = -V_{dc} I_{dc}.$$

or

$$P_{rf} + P_{dc} = 0 \qquad \text{B-2}$$

According to B-2, when the bias circuit supplies power to the junction, the power is radiated by the junction at the frequency ω_0. When the biasing circuit is absorbing power ($I_{dc} V_{dc} < 0$) this power is supplied by the rf power in the junction.

APPENDIX C

CORRECTIONS TO THE WS THEORY

We will consider here the first order corrections to the (W S) assumption of a monochromatic rf voltage in the junction driven resonator. It is easy to show that only harmonics of the Josephson frequency affect the junction properties. Therefore let us assume

$$\int^t \Omega(t')dt' = \xi_1 \sin(\omega t + \phi_1) + \xi_n \sin(n\omega t + \phi_n) \qquad \text{C-1}$$

The nth harmonic amplitude can be calculated from the amplitude of the harmonic of the Josephson fundamental frequency. This is

$$\left[\frac{d^2}{dt^2} + \gamma \frac{d}{dt} + \omega_c^2\right] \xi_n \sin(n\omega t + \phi_n) = A\, \mathcal{I}_{n\omega}(t) \qquad \text{C-2}$$

where

$$\mathcal{I}_n(t) = J_{n-1} \cos(n\omega t + n\phi_1 - \phi_1) + (-1)^{n+1} J_{n+1} \cos(n\omega t + n\phi_1 + \phi_1)$$

where $J_m = J_m(\xi_1)$. Using a bit of trigonometry, we find that $I_{n\omega}(t) = \mathcal{I}_n(\xi_1, \phi_1) \cos(n\omega t + N\phi_1 + \chi_n(\xi_1, \phi))$

where

$$\mathcal{I}_n = \left[(J_{n-1} + (-1)^{n+1} J_{n+1})^2 \cos^2\phi_1 + (J_{n-1} - (-1)^{n+1} J_{n+1})^2 \times \sin^2\phi_1\right]^{1/2} \qquad \text{c-3a}$$

$$\tan\chi_n = -\frac{J_{n-1} - (-1)^{n+1} J_{n+1}}{J_{n-1} + (-1)^{n+1} J_{n+1}} \tan\phi_1 \qquad \text{C-3b}$$

and $J_n \equiv J_n(\xi_1)$.

Putting all this into (C-2) gives

$$\xi_n \cos(n\omega t + \phi_n + \theta_n) = \Gamma_n \cos\theta_n \, \mathcal{U}_n(\xi, \phi_1) \cos(n\omega t + n\phi_1 + X_n)$$

where $\Gamma_n = A/n\gamma\omega$ and $\tan\theta_n = (n^2\omega^2 - \omega_c^2)/n\gamma\omega$. Since this equation is valid for all times, we may equate both amplitudes and phases:

$$\xi_n = \Gamma_n \cos\theta_n \, \mathcal{U}_n(\xi_1, \phi_1) \qquad \text{C-4a}$$

$$\text{and} \qquad \phi_n + \theta_n = N\phi_1 + X_n \qquad \text{C-4b}$$

We may use the unperturbed solution to remove the dependences on ϕ_1. Before that, however, let us calculate the new equation for ξ_1. If we let $\alpha_n \quad n\phi_1 - \phi_n$ we can show that the current at the fundamental is

$$\begin{aligned} I_\omega(t) = {} & J_0 \cos(X - \phi_1) + J_2 \cos(X + \phi_1) + 1/2\, \xi_n \Big\{ (-1)^n \times \\ & [J_n \cos(X + \phi_1 - \alpha_n) + J_{n+2} \cos(X + \phi_1 + \xi_n)] \\ & - [J_n \cos(X + \xi_n - \phi_1) + J_{n-2} \cos(X + \phi_1 - \alpha_n)] \Big\} \end{aligned} \qquad \text{C-5}$$

where we have used $J_1(\xi_n) = -J_{-1}(\xi_n) \cong 1/2\, \xi_n$ since $\xi_n \ll 1$. We can find the new operating point equation by equating C-5 to

$$[d^2/dt^2 + \gamma^d/dt + \omega_c^2] \quad \xi \sin(\omega t + \phi_1).$$

This gives

$$\xi \cos(X + \theta_1) = I_\omega(t)\, \Gamma \cos\theta_1 \qquad \text{C-6}$$

where θ_1, Γ are given in (33) and (34). The perturbed solutions become very complex and no single analytical expression may be given. We can make further progress by assuming that we have tuned the Josephson frequency to the center of the resonance; i.e., $\omega = \omega_c$ so $\theta_1 = 0$ and by (36) $\phi_1 = 0$. In this case from C-4a and C-3a,

$$\xi_n = \Gamma_n \cos\theta_n \, [J_{n-1} + (-1)^{n+1} J_{n+1}] \qquad \text{C-7}$$

$$\xi_1/\Gamma_1 = J_0 + J_2 + 1/2\ \xi_n \left\{(-1)^n [J_n + J_{n+2}] \cos\theta_n - [J_n + J_{n-2}] \cos\theta_n\right\}$$

where we have used $\alpha_n = \theta_n$. Using $J_{n-1} + J_{n+1} = 2n/\xi_1\ J_n$ and putting in (C-7) we get,

$$\xi_1/\Gamma_1 = 2/\xi_1 \left\{J_1 + 1/2\ \Gamma_n \cos^2\theta_n\ [J_{n-1} + (-1)^{n+1} J_{n+1}] \times [(-1)^n J_{n+1}(n+1) - (n-1) J_{n-1}]\right\} \qquad \text{C-8}$$

and finally, the dc current through the junction is, from C-1,

$$I_{dc} = J_{-1}(\xi_1) \cos\phi_1 + \xi_n/2 \left[J_{-n-1} \cos(\phi_n - (n+1)\phi_1) - J_{n-1} \cos((n-1)\phi_1 - \phi_n)\right]$$

Since $\phi_1 = 0$, this becomes

$$I_{dc} = J_1 + \xi_n/2\ [-J_{n-1} + J_{n+1}(-1)^{n+1}] \cos\theta_n$$

where $-\theta_n = \phi_n$. The total dc current using (C-8) and (C-7) is

$$I_{dc} = \xi_1^2/2\Gamma_1 = 1/2\ \Gamma_n \cos^2\theta_n\ n\ [(-1)^n J_{n+1} - J_{n-1}]^2$$

Now we can sum this expression over all n to give

$$I_{dc} = \xi_1^2/2\Gamma_1 - 1/2 \sum_{n>1} n\,\Gamma_n \cos^2\theta_n\ [J_{n-1} - (-1)^n J_{n+1}]^2 \qquad \text{C-9}$$

which is, to within a sign the result quoted in Ref. 29, with the correction that ξ must satisfy (C-8) instead of (35), (or at least the first term in (C-9) - the second term can use (35)).

We see that, from (C-7), the amplitude of the nth harmonic voltage scales with $\Gamma_n \cos\theta_n$. Using $\Gamma_n = 1/n\ \Gamma_1$ we can show that if $\gamma = \omega_c/Q$

$$\Gamma_n \cos\theta_n = \frac{\Gamma_1}{\sqrt{n^2 + Q^2(n^2-1)^2}}$$

or, for $Q \gg 1$

$$\Gamma_1 \cos \theta_n \approx \frac{\Gamma_1}{Q(n^2-1)} \qquad \text{C-10}$$

The harmonic effects on the implicit equation for ξ_1, however, goes as $\Gamma_n \cos^2 \theta_n$, and for $Q \gg 1$

$$\Gamma_n \cos Q_n \approx \Gamma_1 \frac{n}{Q^2(n^2-1)^2} \qquad \text{C-11}$$

We can replace (C-8) with

$$\xi_1/\Gamma_1 = 2/\xi_1 \approx \left[J_1 - \Gamma_1/Q^2 \, K(\xi_1)\right] \qquad \text{C-12}$$

where

$$K(\xi) = \sum_{n \geq 2} \frac{n}{(n^2-1)^2} \left[(-1)(n+1) J_{n+1} - (n-1) J_{n-1}\right]$$

$$\times \left[(-1)^n J_{n+1} - J_{n-1}\right]$$

It is relatively easy to show that $K(\xi) \geq 0$, so that the presence of the harmonics reduces the operating point value of ξ_1. For $\Gamma_1 > 2.91$, the rf voltage, ξ_1 still saturates. The presence of the correction terms in (C-12) only requires a somewhat larger value of Γ_1. viz: For $\Gamma_1 > 2.91$, $K(\xi_1)$ is constant and equal to $K(1.841)$ and C-12 becomes

$$\xi_1/\Gamma_1 + \Gamma_1/Q^2 \; K(1.841) = 2/\xi_1 \, J_1 \qquad \text{C-13}$$

which still forces ξ_1 to saturate at 1.841.

ACKNOWLEDGEMENTS

The author wishes to thank Professor P. L. Richards for his initial suggestion of research project and continued guidance and encouragement. Much of the work in this thesis would be absent but for his efforts. The author also acknowledges the fruitful results of many discussions with Professors J. Clarke and G. I. Rochlin. Most of all, the author must give thanks for the unflagging enthusiasm and emotional support of his wife, Karen Kramer Sterling, to whom this work must be dedicated.

This work was supported in part by the United States Atomic Energy Commission.

REFERENCES

1. J. E. Zimmerman and A. H. Silver, Phys. Letters 10, 49 (1966).

2. For a comprehensive review, see R. de Bruyn Ouboter and A. Th. A. m. de Waele, Progress in Low Temperature Physics, Vol VI, C. J. Gorter, ed., (North Holland Publishing Co., Amsterdam, to be published).

3. C. C. Grimes, P. L. Richards and S. Shapiro, Phys. Rev. Letters 17, 431 (1966).

4. C. C. Grimes, P. L. Richards, and S. Shapiro, J. Appl. Phys. 8, 3905 (1968).

5. C. C. Grimes and S. Shapiro, Phys. Rev. 169, 397 (1968).

6. W. H. Parker, D. N. Langenberg, A. Denenstein, and B. N. Taylor, Phys. Rev. 177, 639 (1969).

7. A. H. Silver and J. E. Zimmerman, Appl. Phys. Letters 10, 142 (1967).

8. P. L. Richards and S. A. Sterling, Appl. Phys. Letters 14, 394 (1969).

9. See for example P. G. DeGennes, Superconductivity in Metals and Alloys (W. A. Benjamin, Inc., New York; 1966).

10. H. Kamerlingh Onnes, Comm. Phys. Lab. Univ. Leiden, Nos. 119, 120, 122 (1911).

11. W. Meissner and R. Ochsenfeld, Naturwiss. 21, 787 (1933).

12. F. London and H. London, Proc. Roy. Soc., A149, 71 (1935).

13. F. London, Phys. Rev 74, 562 (1948).

14. C. J. Gorter and H. G. B. Casimer, Phys. Z. 35, 963 (1934); Z. Techn. Phys. 15, 539 (1934).

15. V. L. Ginsberg and L. D. Landau, Zh. Eksperim i Theor. Fiz. 20, 1064 (1950).

16. J. Bardeen, L. N. Cooper and J. R. Schrieffer, Phys. Rev. 108, 1175 (1957).

17. Bernhard Muhlschegel, Z. Physik 155, 313 (1959).

18. L. P. Gorkov, Zh, Eksperim. i Teor. Fiz. 36, 1918 (1959); (English transl., Soviet Phys. - JETP 9, 1364 (1959).

19. D. H. Douglass and L. M. Falicov, Progress in Low Temperature Physics Vol. IV, C. J. Gorter (ed)., (North Holland Publishing Co., Amsterdam, 1963).

20. I. Giaever, Phys. Rev. Letters 5, 147 464 (1960).

21. B. D. Josephson, Phys. Letters 1, 251 (1962).

22. C. S. Owen and D. J. Scalapino, Phys. Rev. 164, 164 (1967).

23. P. W. Anderson and J. M. Rowell, Phys. Rev. Letters 10, 230 (1963).

24. S. Shapiro, Phys. Rev. Letters 11, 80 (1963).

25. D. N. Langenberg, D. J. Scalapino, B. N. Taylor and R. E. Eck, Phys. Rev. Letters 15, 294 (1965).

26. A. H. Dayem and C. C. Grimes, Appl. Phys. Letters 9, 47 (1966).

27. J. E. Zimmerman, J. A. Cowan and A. H. Silver, Appl. Phys. Letters 9, 353 (1966).

28. Viany Ambegaokar and Alexis Baratoff, Phys. Rev. Letters 10, 486 (1963).

29. N. R. Werthamer, Phys. Rev. 147, 255 (1966).

30. E. Riedel, Z. Naturforsch. 19A, 1634 (1964).

31. B. D. Josephson, Rev. Mod. Phys. 36, 216 (1964).

32. P. W. Anderson, Progress in Low Temperature Physics, Vol. V, C. J. Gorter (ed.), (North Holland Publishing Co., Amsterdam, 1967).

33. P. W. Anderson and A. H. Dayem, Phys. Rev. Letters 195 (1964).

34. J. E. Zimmerman and J. E. Mercereau, Phys. Rev. Letters 13, 125 (1964).

35. W. A. Harrison, Phys. Rev. 123, 85 (1961).

36. D. E. McCumber, J. Appl. Phys. 39, 3113 (1968).

37. Vinay Ambegaokar and B. I. Halperin, Phys. Rev. Letters, 22, 1364 (1969); Yu M. Hanchenko and L. A. Zil'berman, Zh. ir Eksperim i Teor. Fiz. 55, 2395 (1968).

38. A. S. Barker, Jr., PhD Thesis, University of Calif.-Berkeley, (1962) (unpublished).

39. See P. L. Richards in Spectroscopic Techniques in Far Infrared, Millimeter, and Submillimeter Waves, D. H. Martin (ed.), (North Holland Publishing Co. Amsterdam, 1967).

40. G. I. Rochlin, Rev. Sci. Inst. (to be published).

41. N. R. Werthamer and S. Shapiro, Phys. Rev. 164, 523 (1967).

42. R. DeBrugn Ouboter, W. H. Kraan, A. Th. A. M. De Waale, and M. H. Omar, Physica 35, 335 (1967).

43. E. H. Putley, Infrared Phys. 4, 1 (1964).

44. T. D. Clark, Phys. Letters 9, 585 (1968).

45. Supplied by Winsted PrecisionBall Corp,; Winsted, Conn., 06098.

Figure Captions

Fig. 1 Frequency dependence of the response of the zero-voltage dc Josephson current. The response is given by $j(\omega) = 1/2\ \mathrm{Re}\left\{j_2(o) + j_2(\omega)\right\}$ and is taken from Ref. 29.

Fig. 2 Schematic representation of a single point contact. The vertical scale is much accentuated.

Fig. 3 Upper: Current-Voltage characteristic of ideal Josephson junction shunted by a unit conductance.

Lower: Responsivity of ideal junction to a change in critical current at constant bias current.

Fig. 4 Current-Voltage characteristic of a tantalum-tantalum point contact junction at 2.69°K.

Fig. 5 Interferogram of the response of a niobium-niobium point contact junction at 4.2°K in the geometry of Fig. 7D. The response peak is at $\nu = 8.50\ \mathrm{cm}^{-1}$ with a line width $\Delta\nu = 0.28\ \mathrm{cm}^{-1}$.

Fig. 6 Point contact holder. S_1 = superconducting post; S_2 = superconducting point; I = insulating point holder; C = contact screw and electrode; D = Differential screw; N = pivoting nuts; L = far infrared light pipe; and F = focusing cone. The holder is 3 inches high.

Fig. 7 Typical resonator geometries. In all cases, the far infrared radiation enters the resonator via the focusing cone at the top of each resonator.

Fig. 8 Biasing circuit for junction. C_1 = dc blocking capacitor; T_1 = isolation transformer; R_s = current shunt resistor; R_I = current measuring resistor; and T_2 = variable gain transformer.

Fig. 9 Graphic solutions to equation (35). The curves at the right are exploded view of system near saturation. The curves are $\mathcal{J}_1(\xi,\theta)\cos\theta=$ ac current in phase with the resonator voltage ξ.

Fig. 10 Normalized resonant response to applied ac voltages. Tan θ = $(\omega^2 - \omega_c^2)/\gamma\omega \simeq (\omega - \omega_c)/\omega_{1/2}$ if $\gamma/\omega << 1$, and the frequency of the applied voltage is assumed equal to Josephson Frequency ω.

Fig. 11 Characteristics of niobium-niobium junction at 4.2°K in resonator C of Fig. 7. Plotted against dc voltage are (a) dc current (with the zero-voltage current compressed)(b) dV/dI = differential resistance, and (c) response to broadband far infrared radiation. Self induced steps occur at 392 μV.

Fig. 12 Characteristics of niobium-niobium junction (same junction as shown in Fig. 11) in weak magnetic field.
Upper: differential resistance, Lower: Response to broadband far infrared radiation. Arrows label self induced steps at 392 μV.

Fig. 13 Spectral response of junction shown in Fig. 12 with dc bias voltage = 350 μV.

Fig. 14 Plot of peak spectral response vs. self induced step voltage associated with the resonant response peak.

Fig. 15 Apparatus for forming multi-junction array. Q = crystal quartz plates, B = electrode, A = adjustment screw, R = reflector.

Fig. 16 Current-voltage characteristic of 0.8 mm Sn bearing array at 2.69°K.

Fig. 17 Characteristics of array of 0.8 mm dia Sn bearings at 1.85°K.
Upper: differential resistance
Lower: Response to broadband radiation.

Fig. 18 Spectral response of Sn array to broadband far infrared radiation.

Fig. 19 Spectral response of Sn array to broadband far infrared radiation at 3.60°K. The two particle energy gap is about 3 cm^{-1}.

Fig. 20 Spectral response of tantalum-tantalum point contact.

Insert: Energy gap from I-V characteristic and spectral response minimum versus reduced BCS gap. $2\Delta(T = 0) = 1.37$ mV, $T_c = 4.30°K$.

Fig. 21 Response sepctra of tantalum-tantalum point contact at 3.905 and 3.297°K.

Fig. 22 Peak response frequency and two-particle energy gap versus BCS reduced gap. $2\Delta(T=0) = 1.38$ mV, $T_c = 4.30°K$.

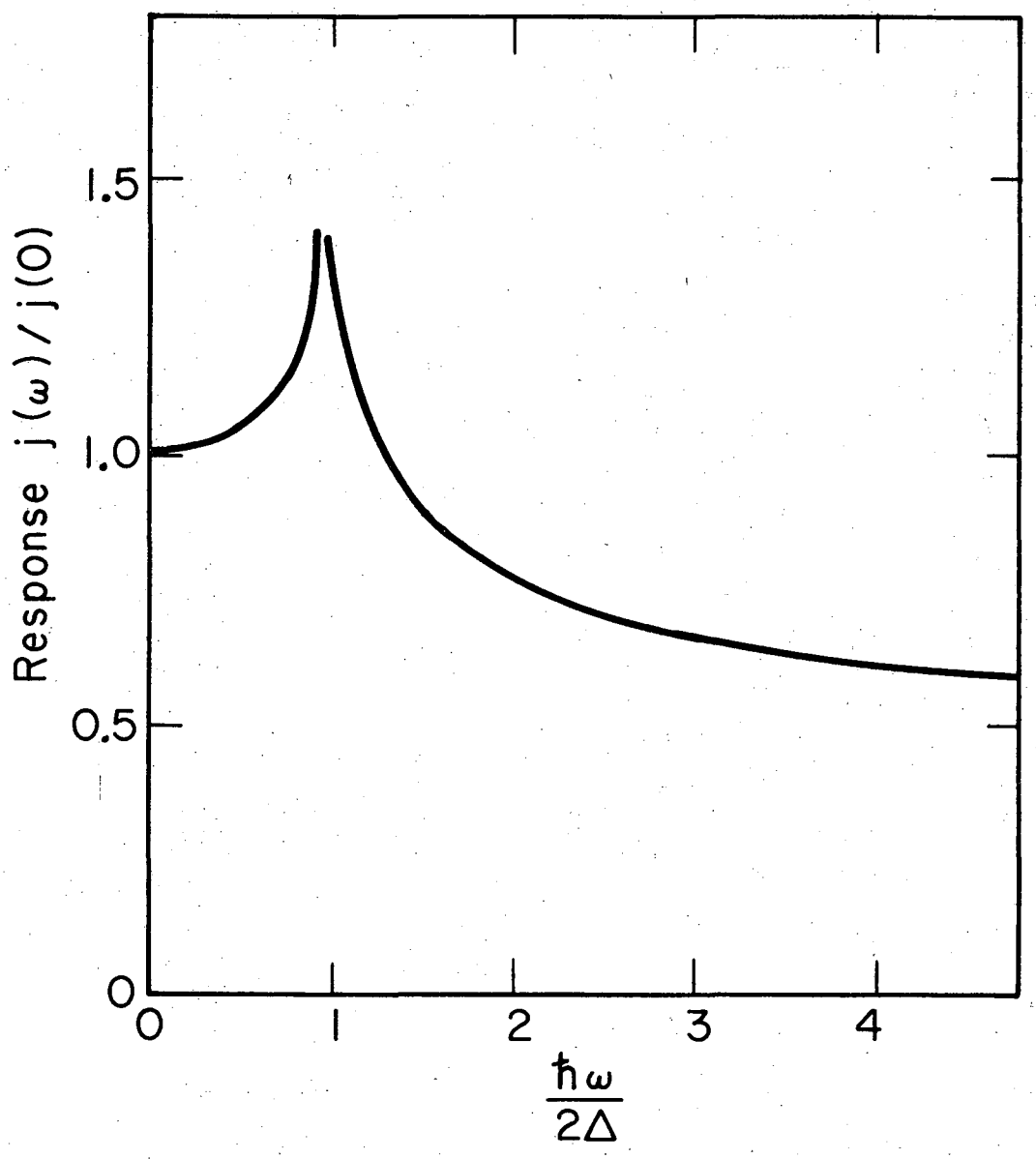

XBL698-3400

Fig. 1

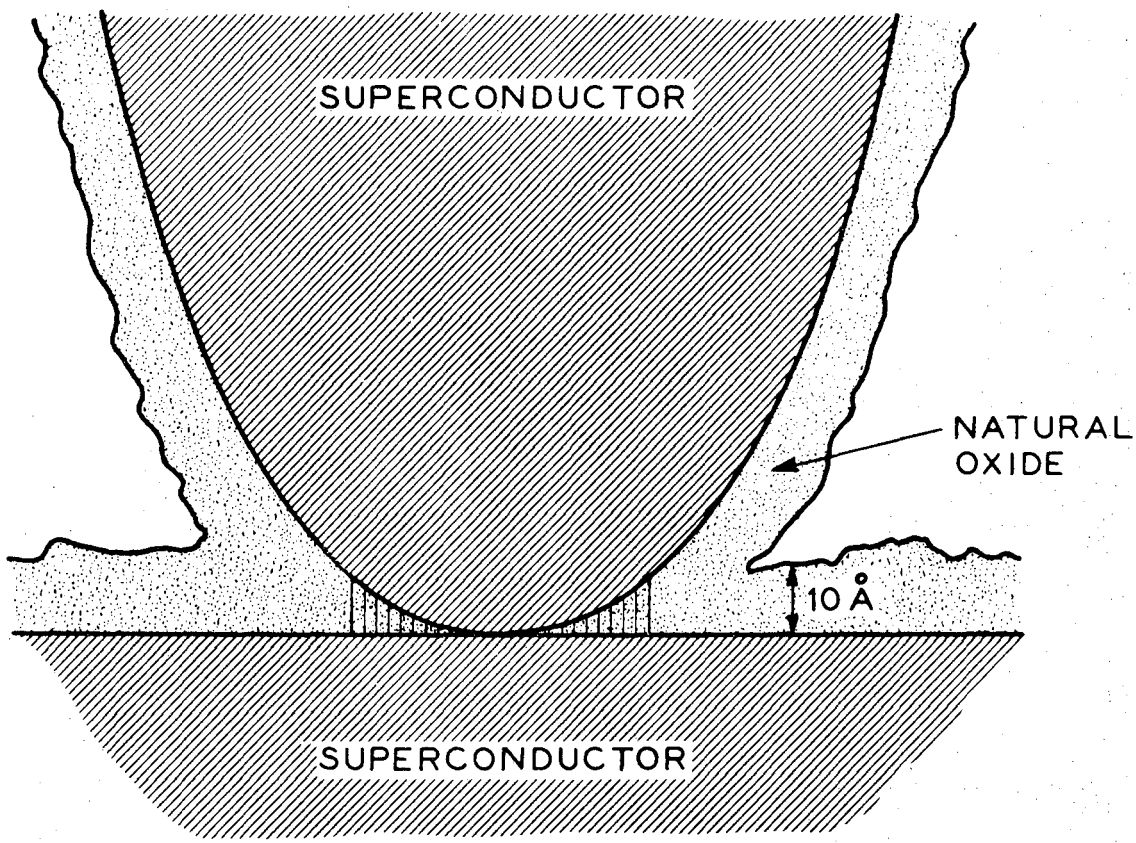

XBL 698-1374

Fig. 2

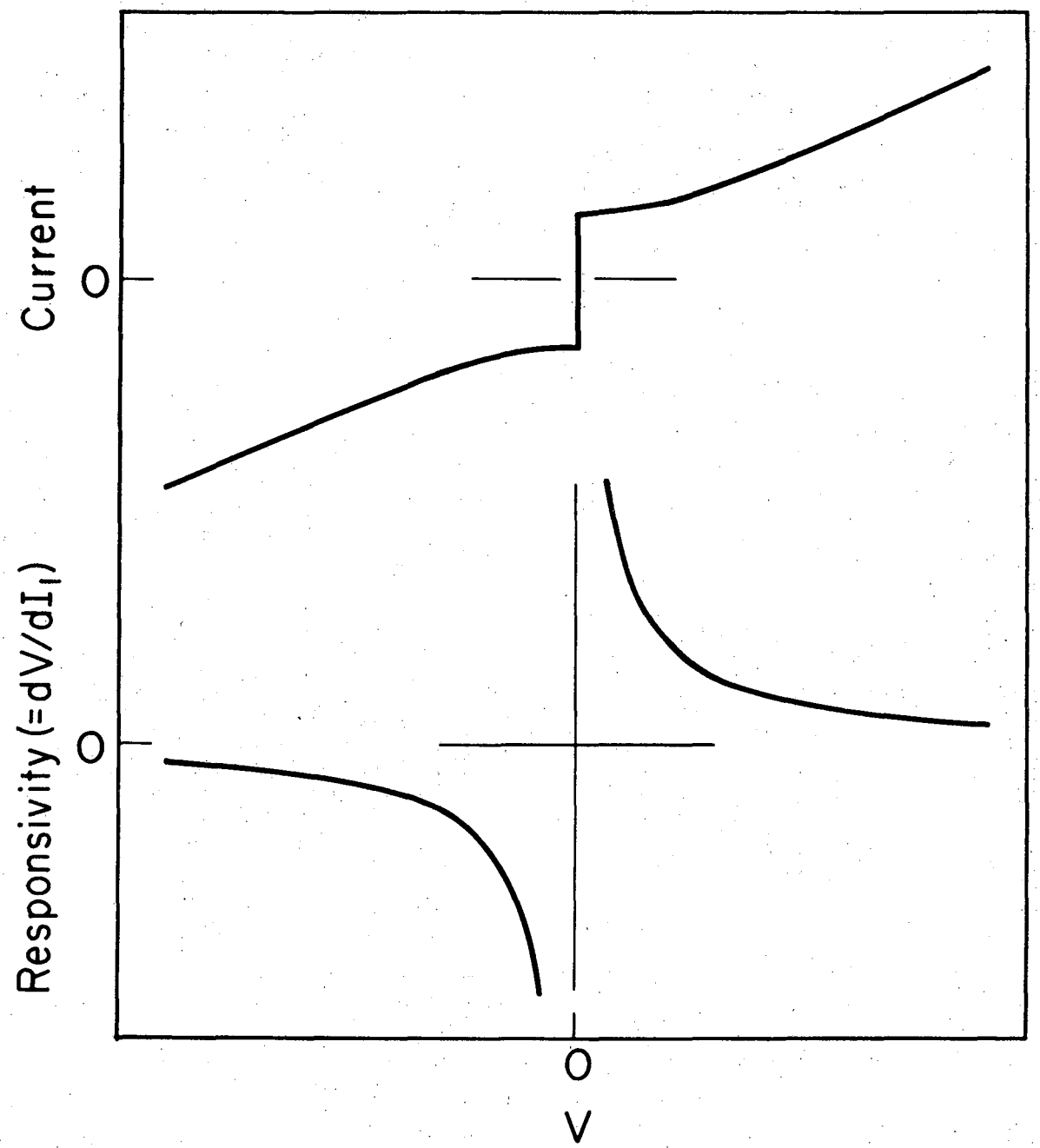

XBL698-3399

Fig. 3

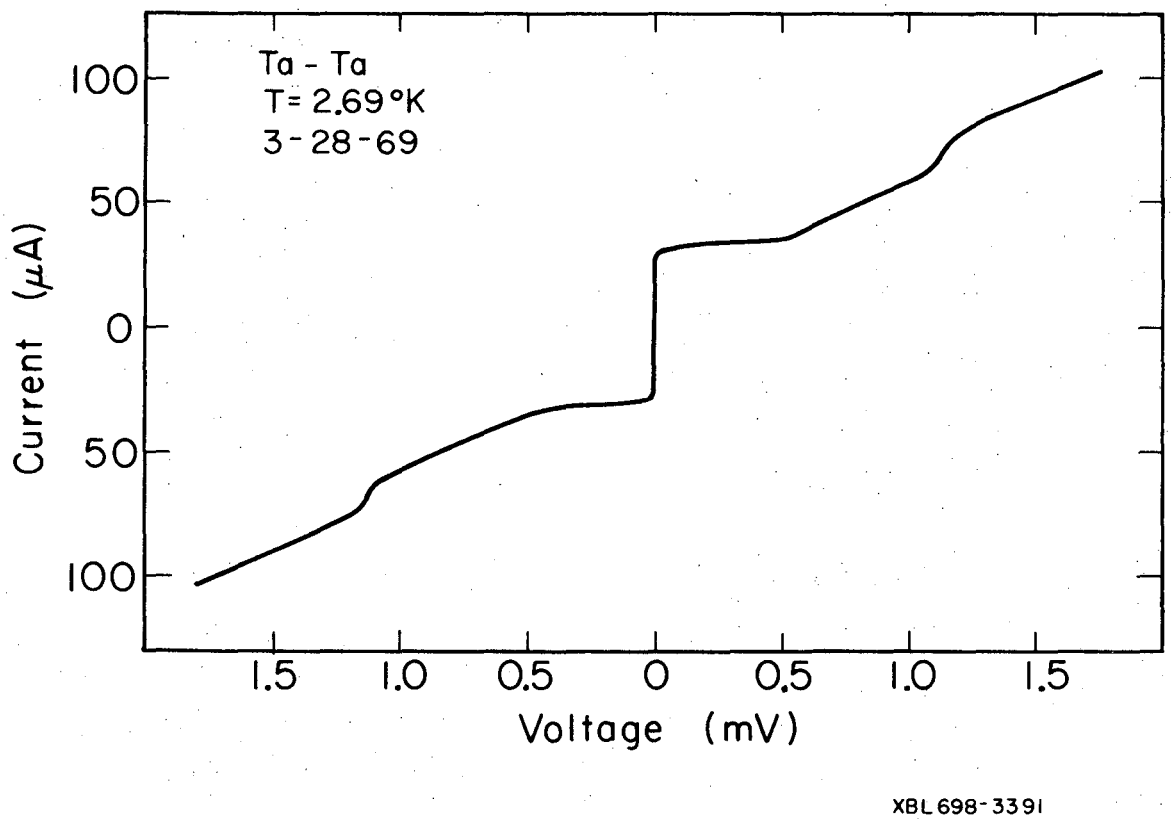
Ta - Ta
T= 2.69°K
3-28-69
100
50
0
50
100
Current (μA)
1.5
1.0
0.5
0
0.5
1.0
1.5
Voltage (mV)
XBL698-3391

Fig. 4

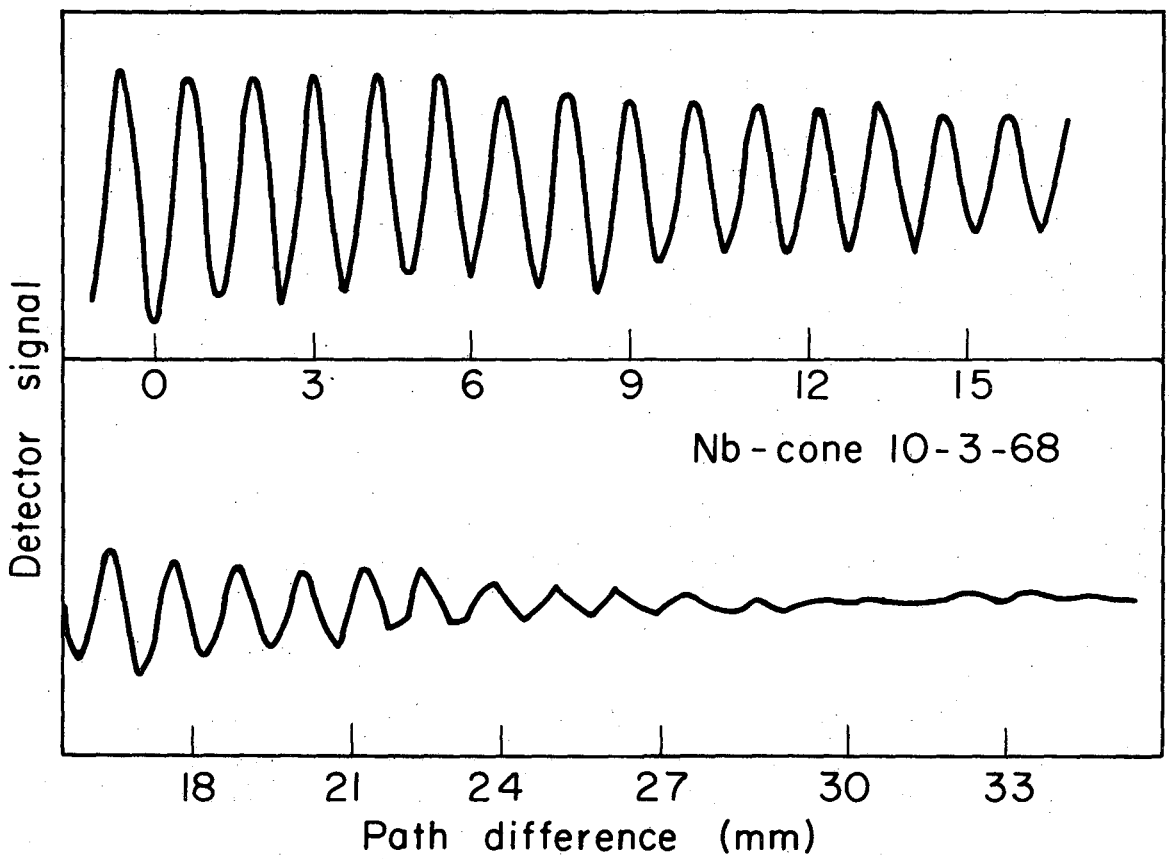

XBL698-3397

Fig. 5

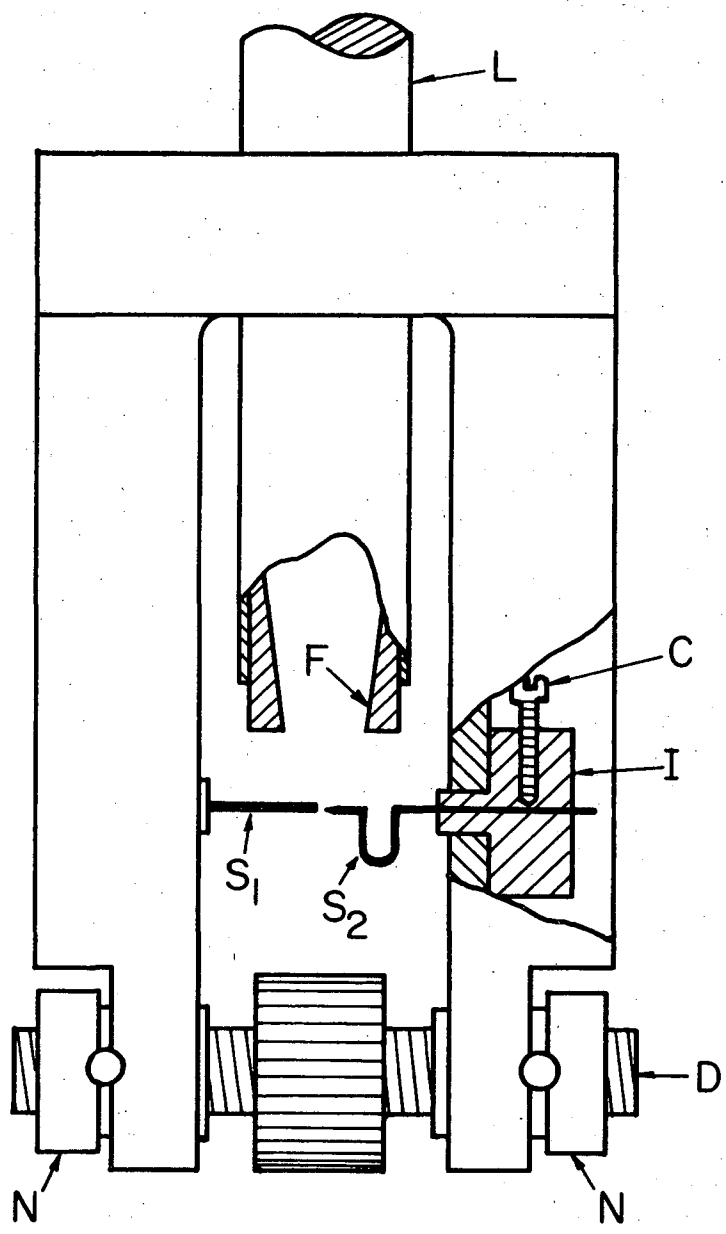

XBL 698-3401

Fig. 6

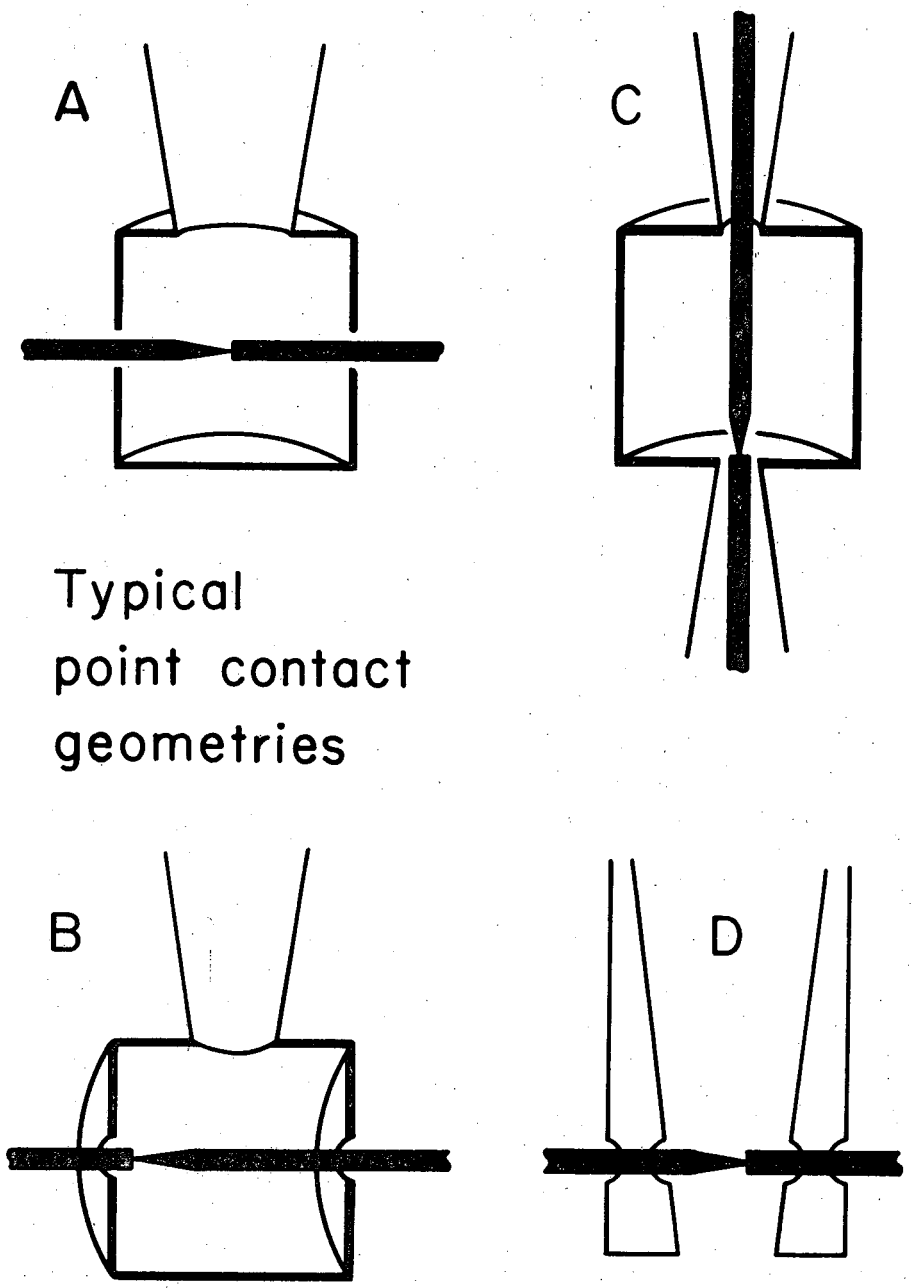

XBL6910-3934

Fig. 7

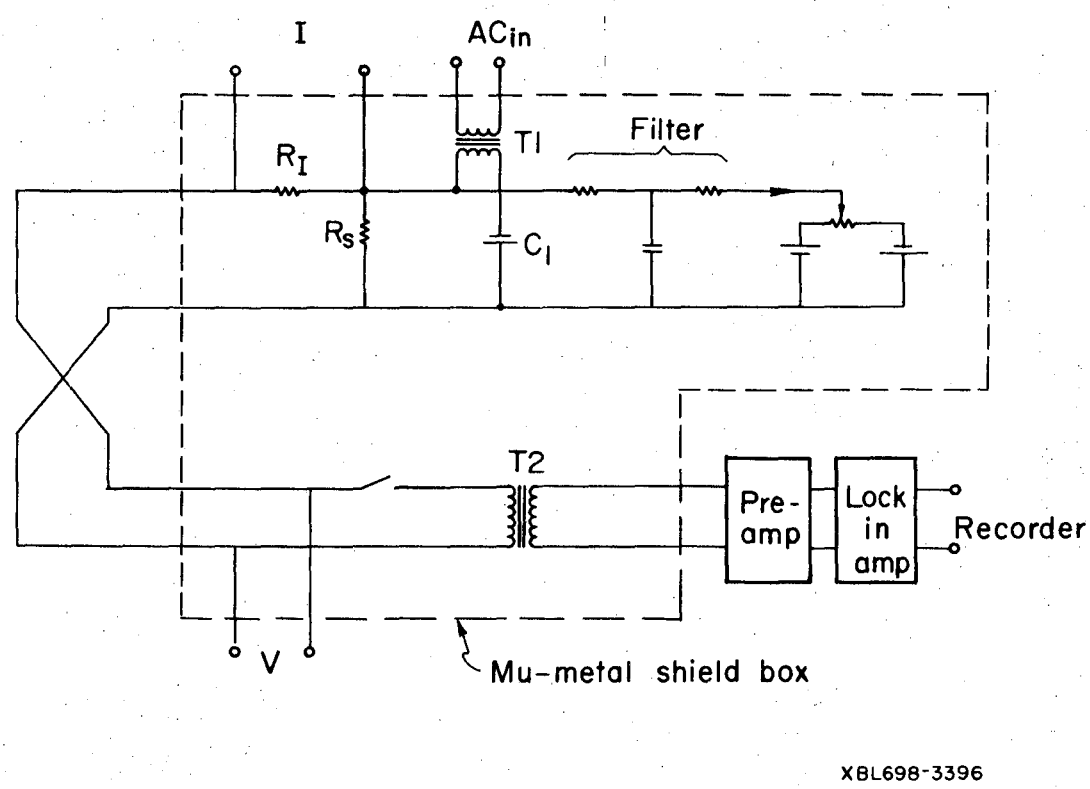
I
ACin
T1
Filter
RI
Rs
C1
T2
Pre-
amp
Lock
in
amp
Recorder
V
Mu-metal shield box
XBL698-3396

Fig. 8

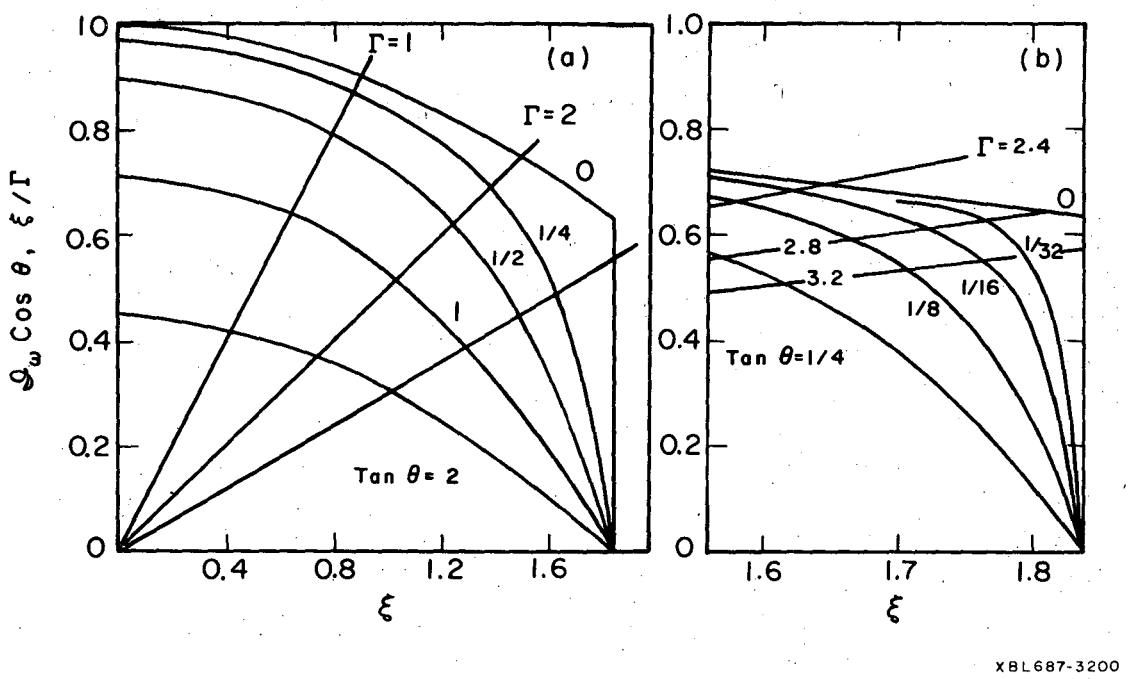
(a)
(b)
Γ=1
Γ=2
0
1/4
1/2
1
Tan θ= 2
Γ=2.4
2.8
3.2
1/32
1/16
1/8
Tan θ=1/4
$\mathcal{J}_\omega$ Cos θ, ξ/Γ
ξ
XBL687-3200

Fig. 9

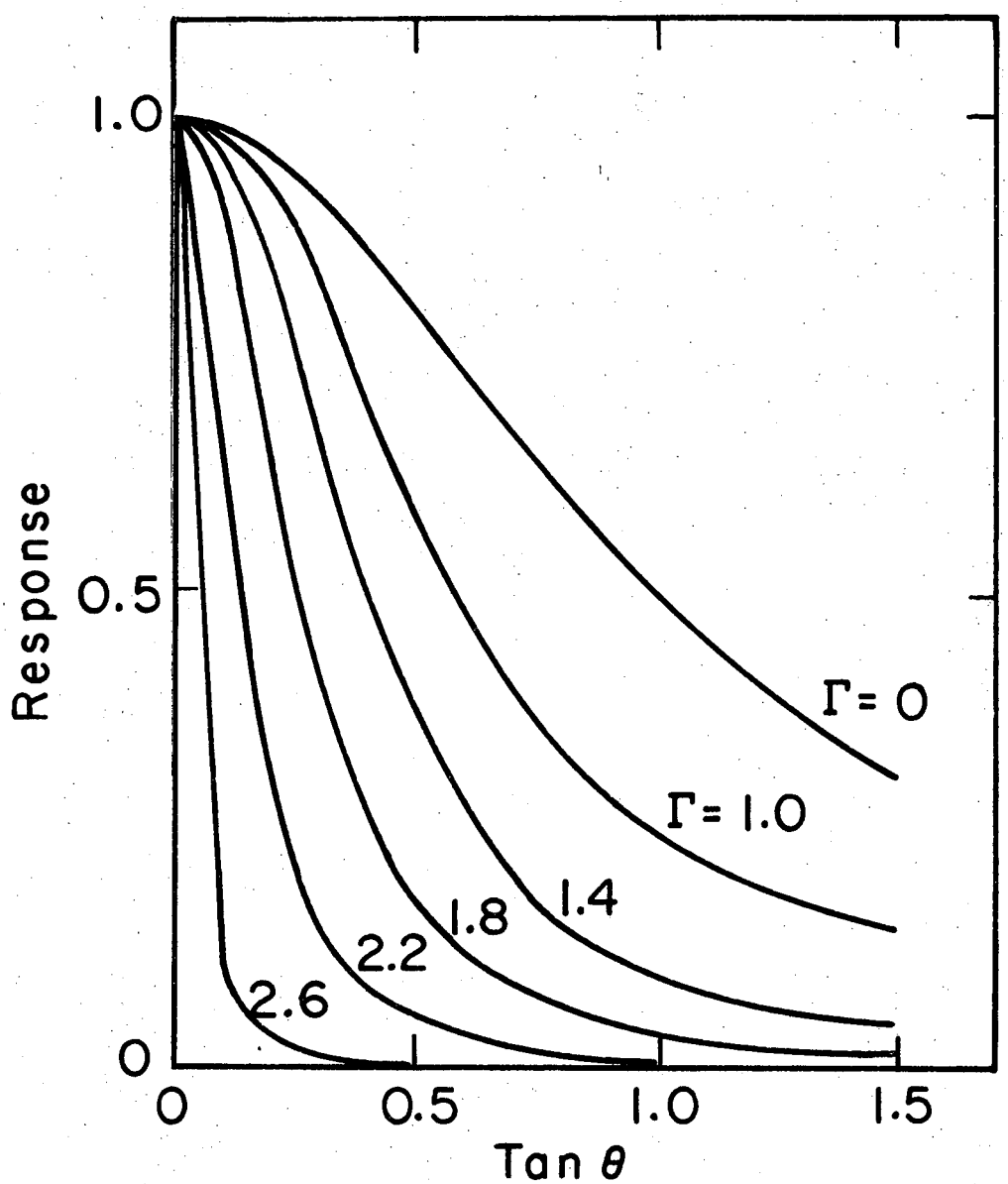

XBL687-3199

Fig. 10

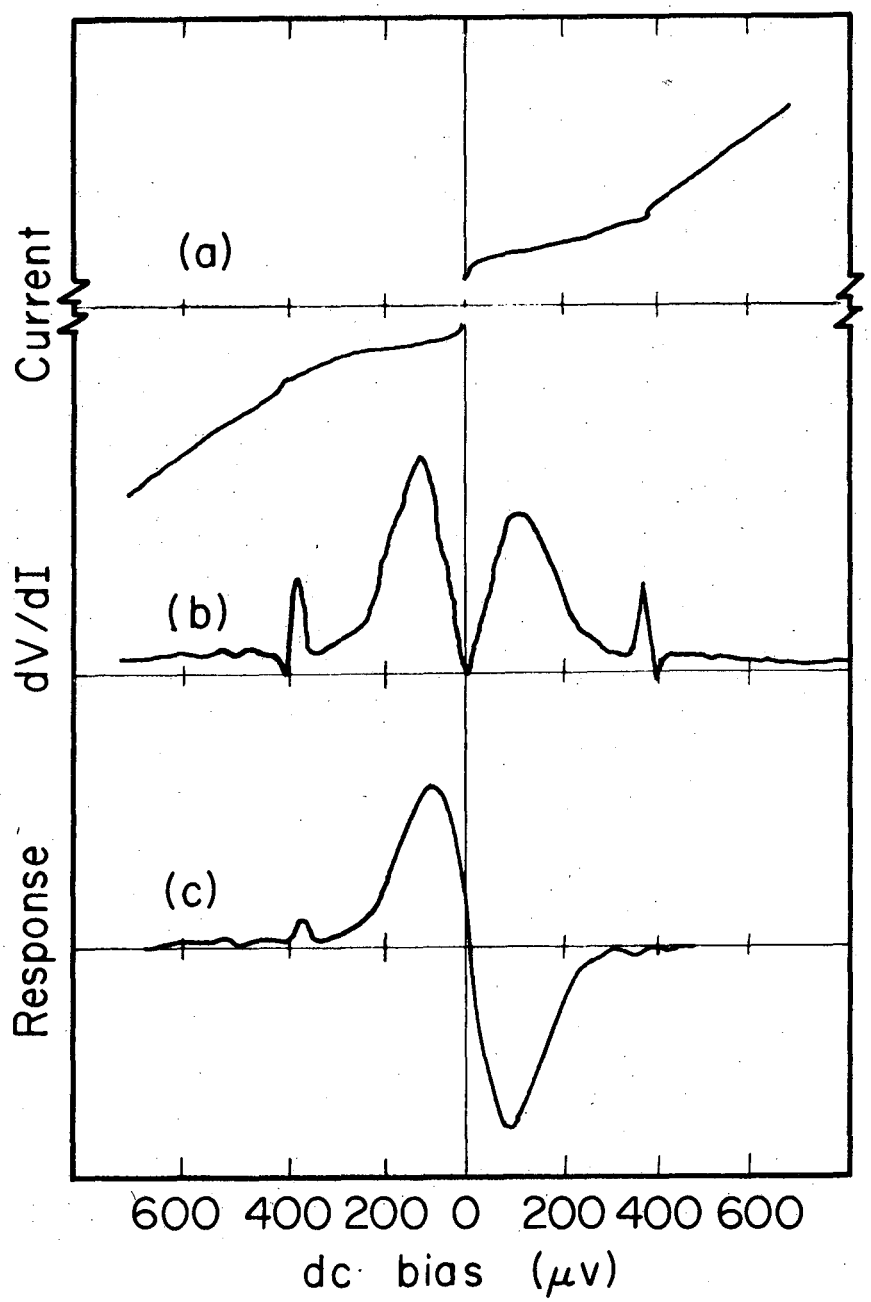

XBL691-1701

Fig. 11

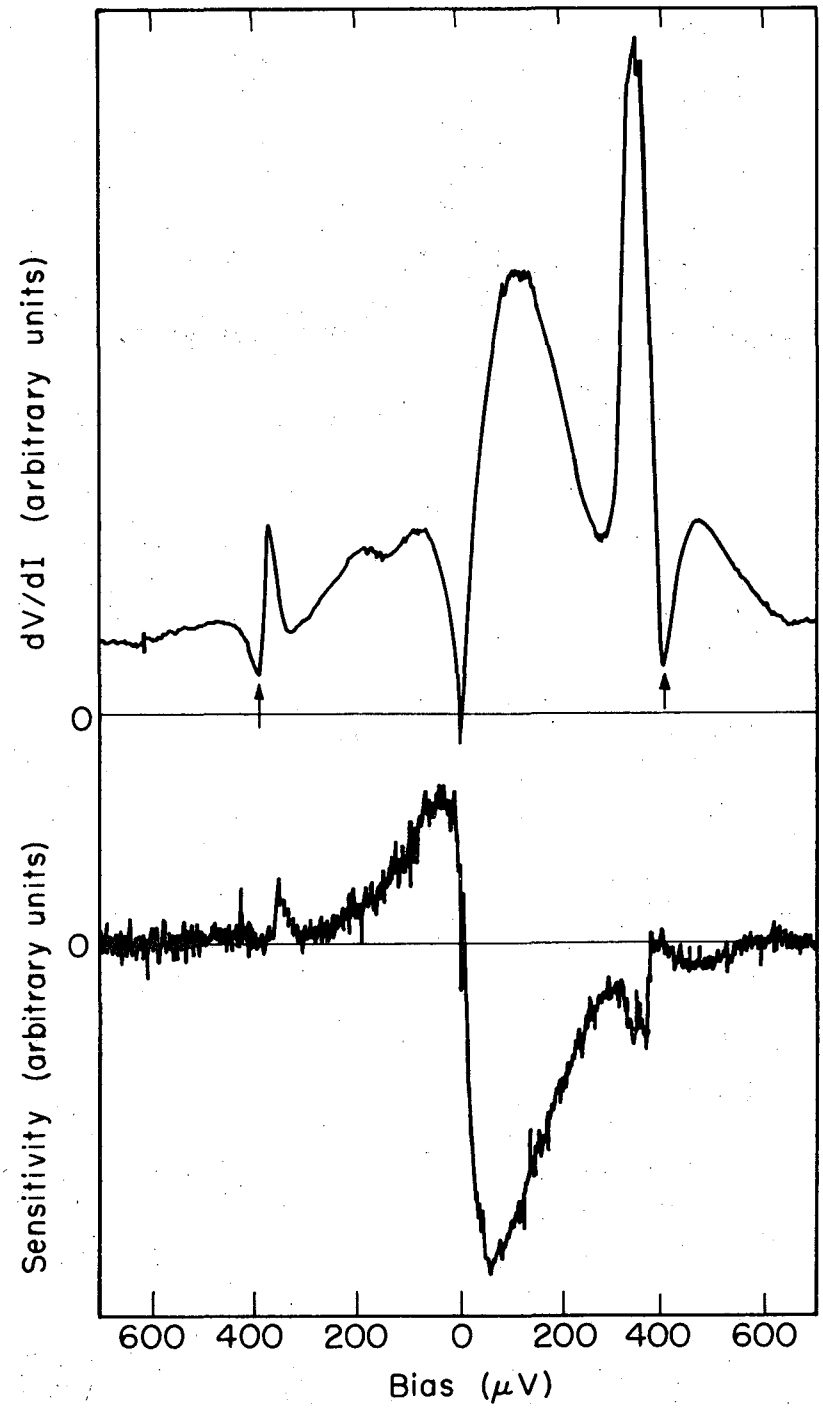

XBL687-3159

Fig. 12

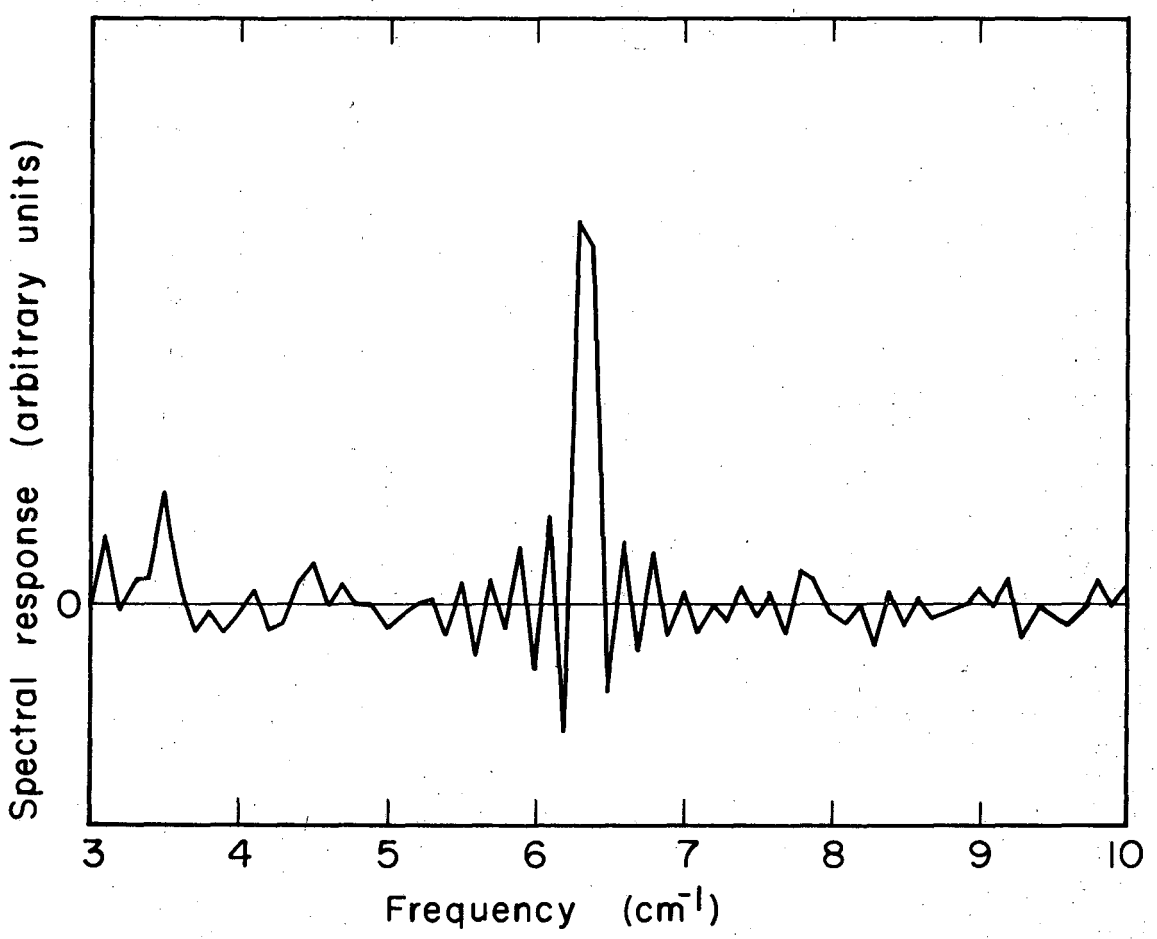

XBL687-3160

Fig. 13

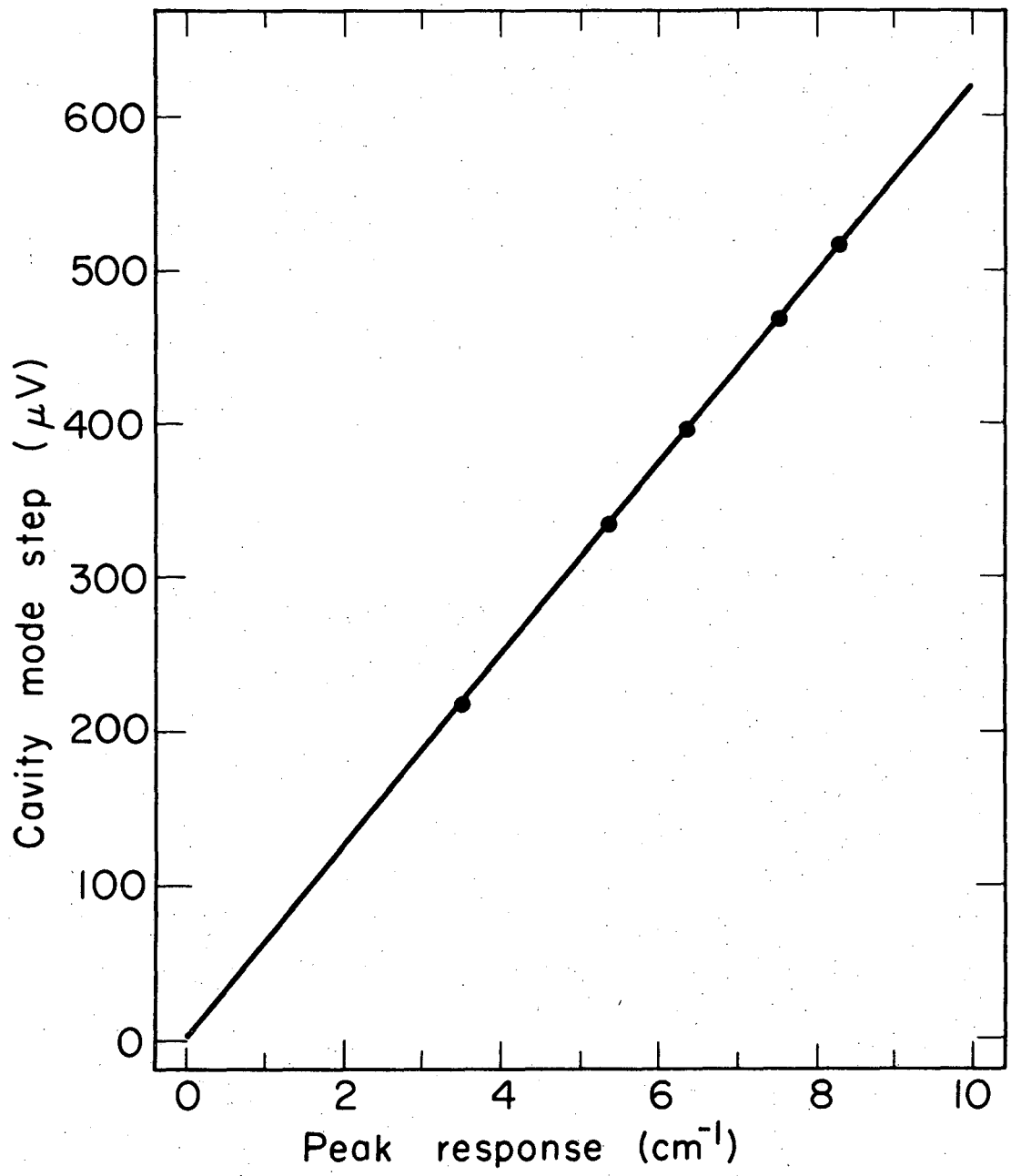

XBL698-3398

Fig. 14

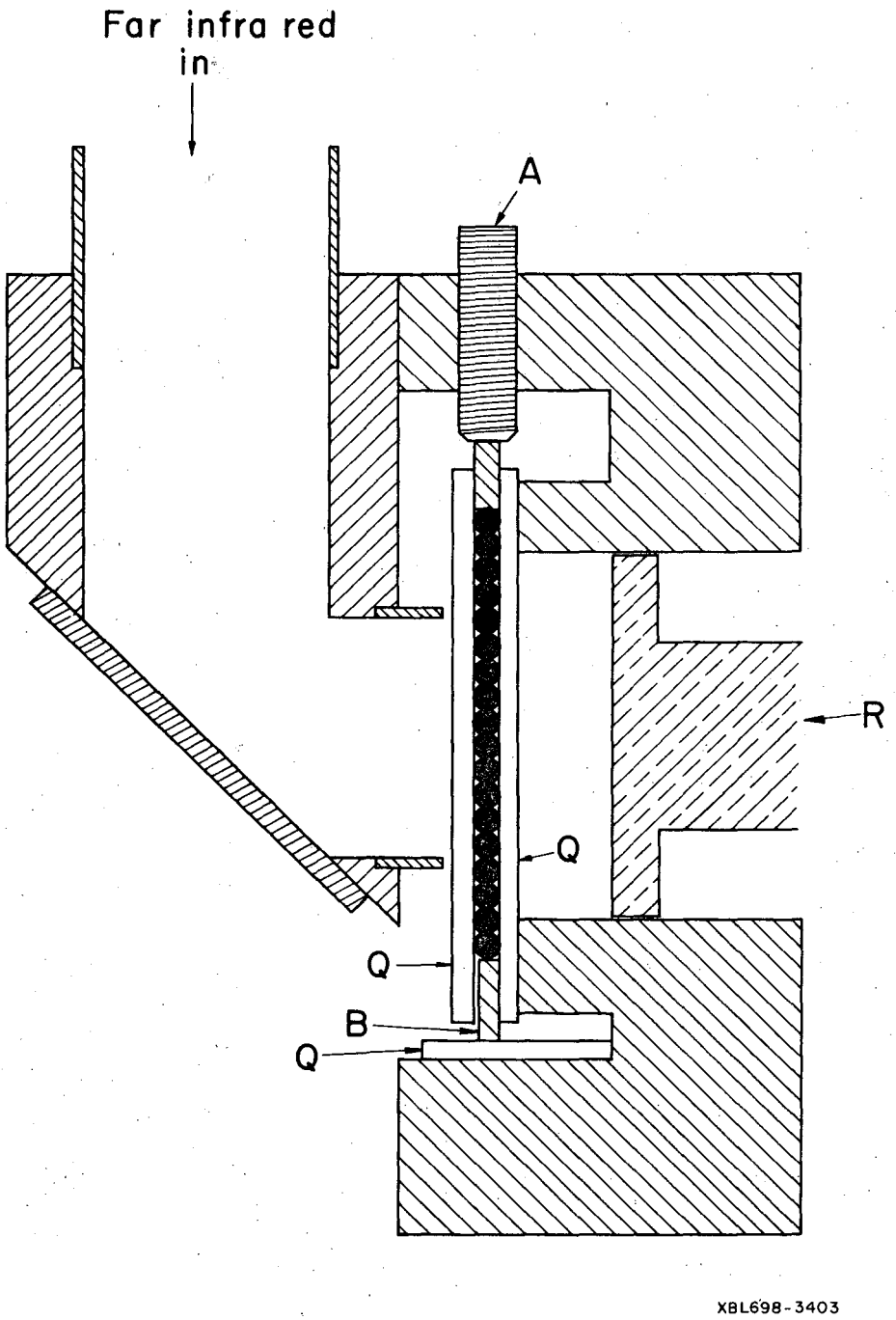

Fig. 15

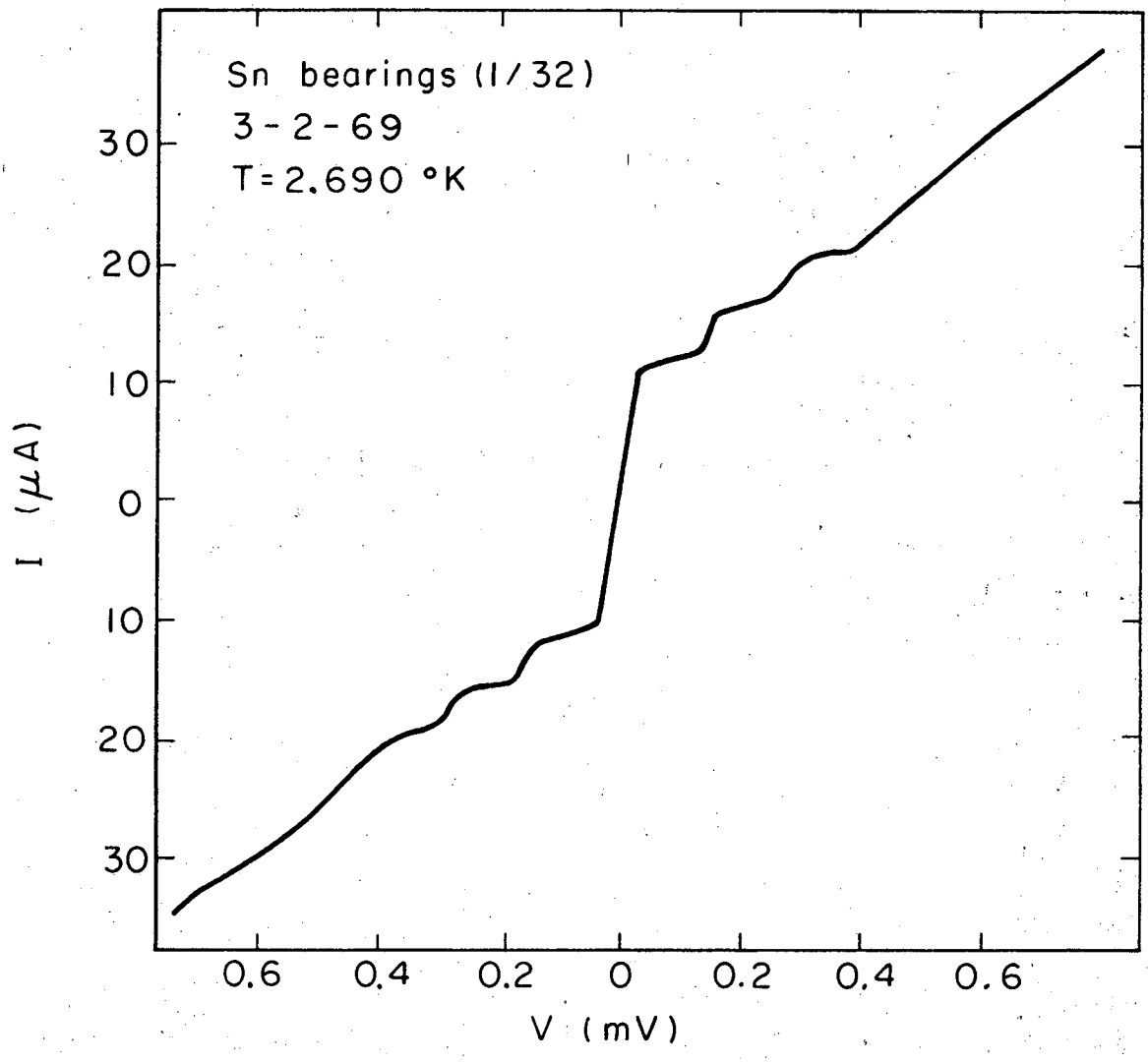

XBL698-3540

Fig. 16

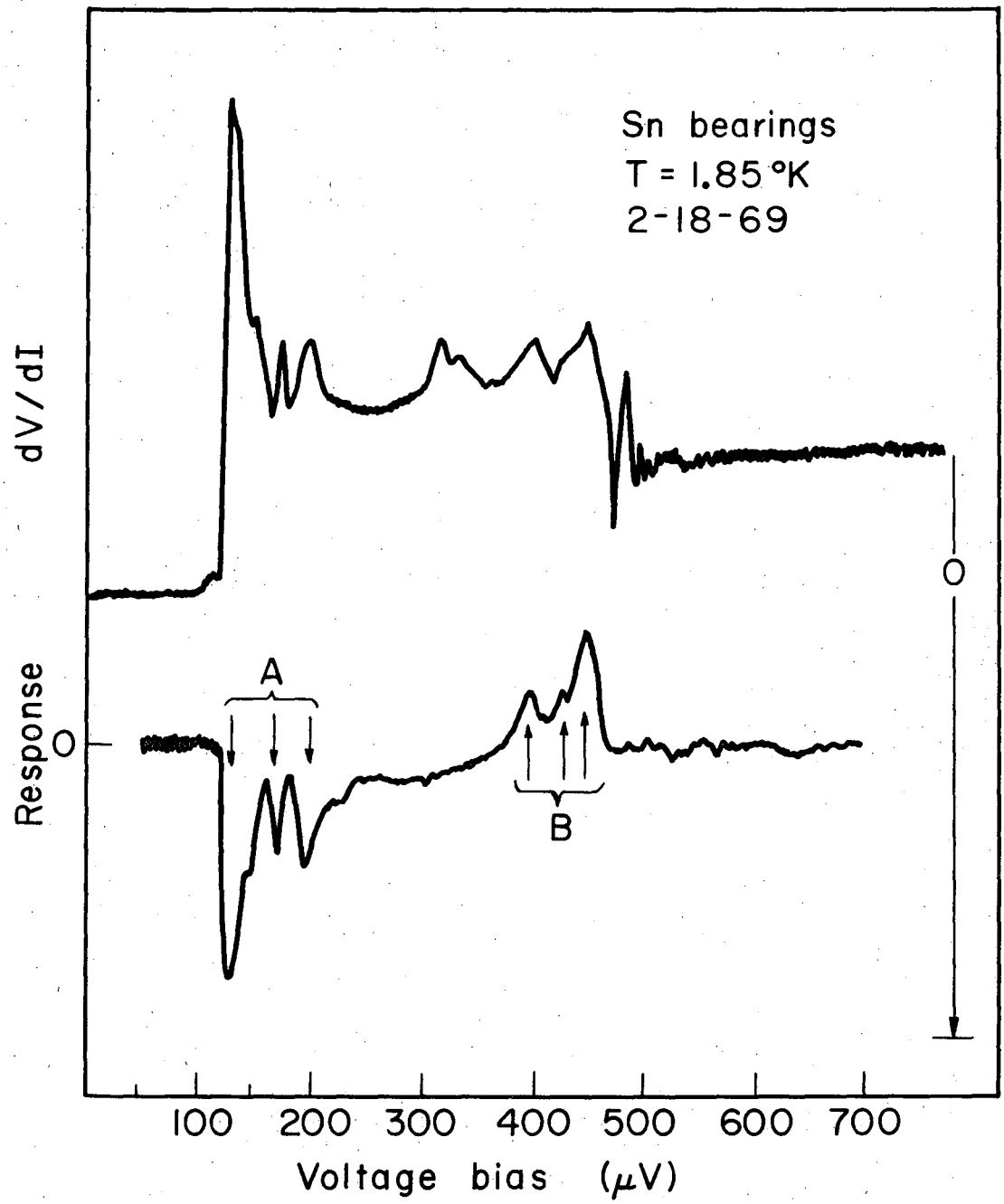

XBL698-3395

Fig. 17

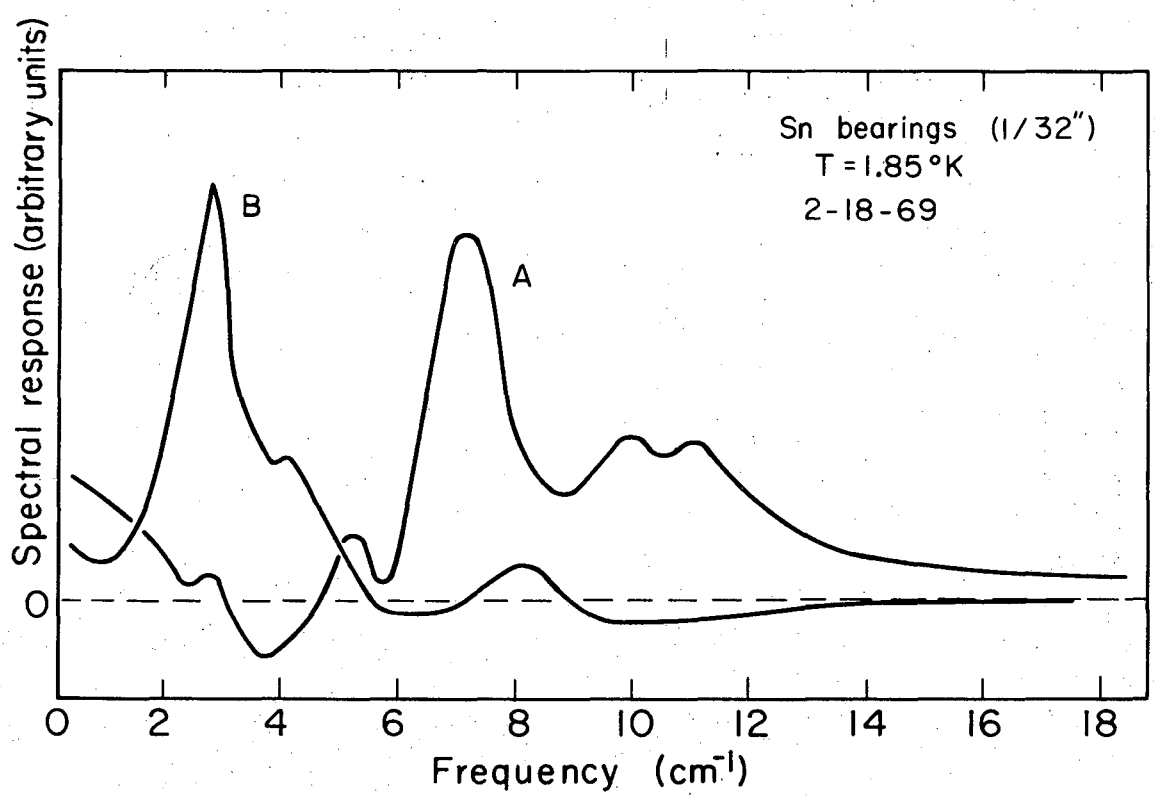

XBL698-3393

Fig. 18

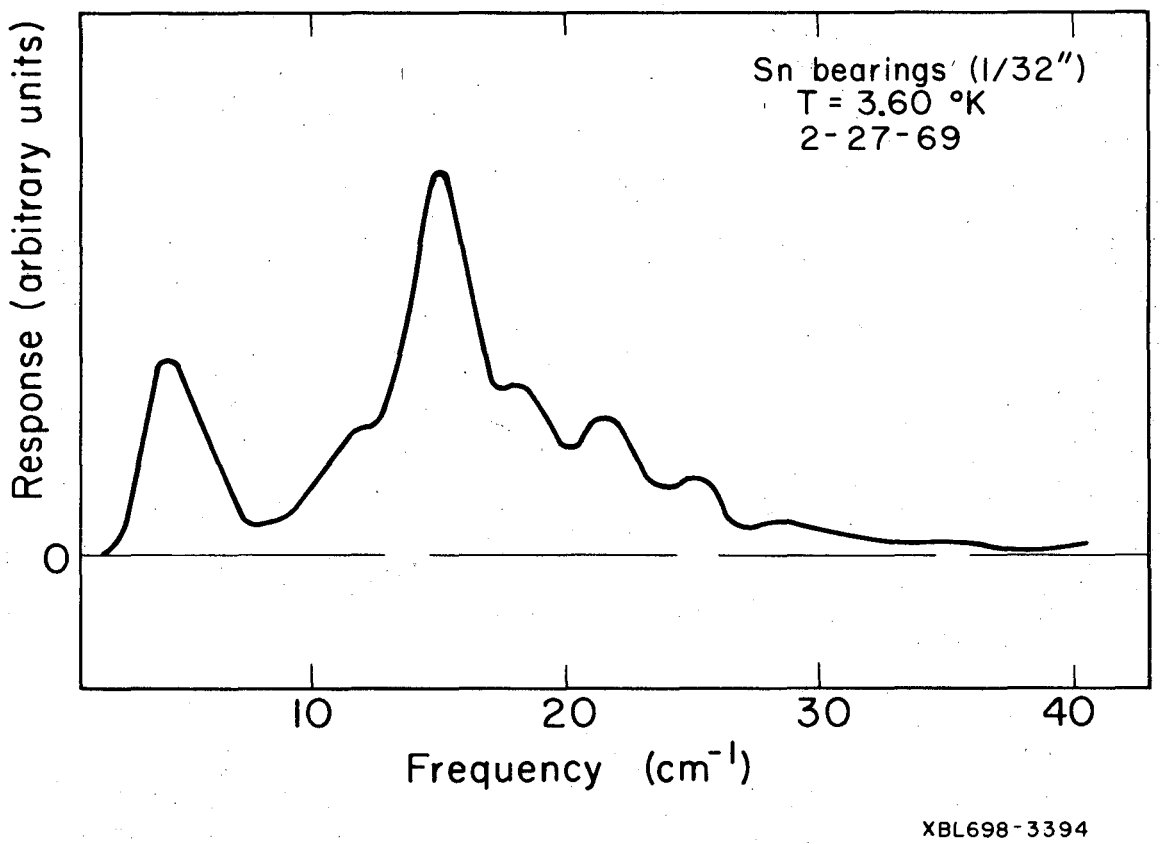
Sn bearings (1/32")
T = 3.60 °K
2-27-69
Response (arbitrary units)
0
10
20
30
40
Frequency (cm⁻¹)
XBL698-3394

Fig. 19

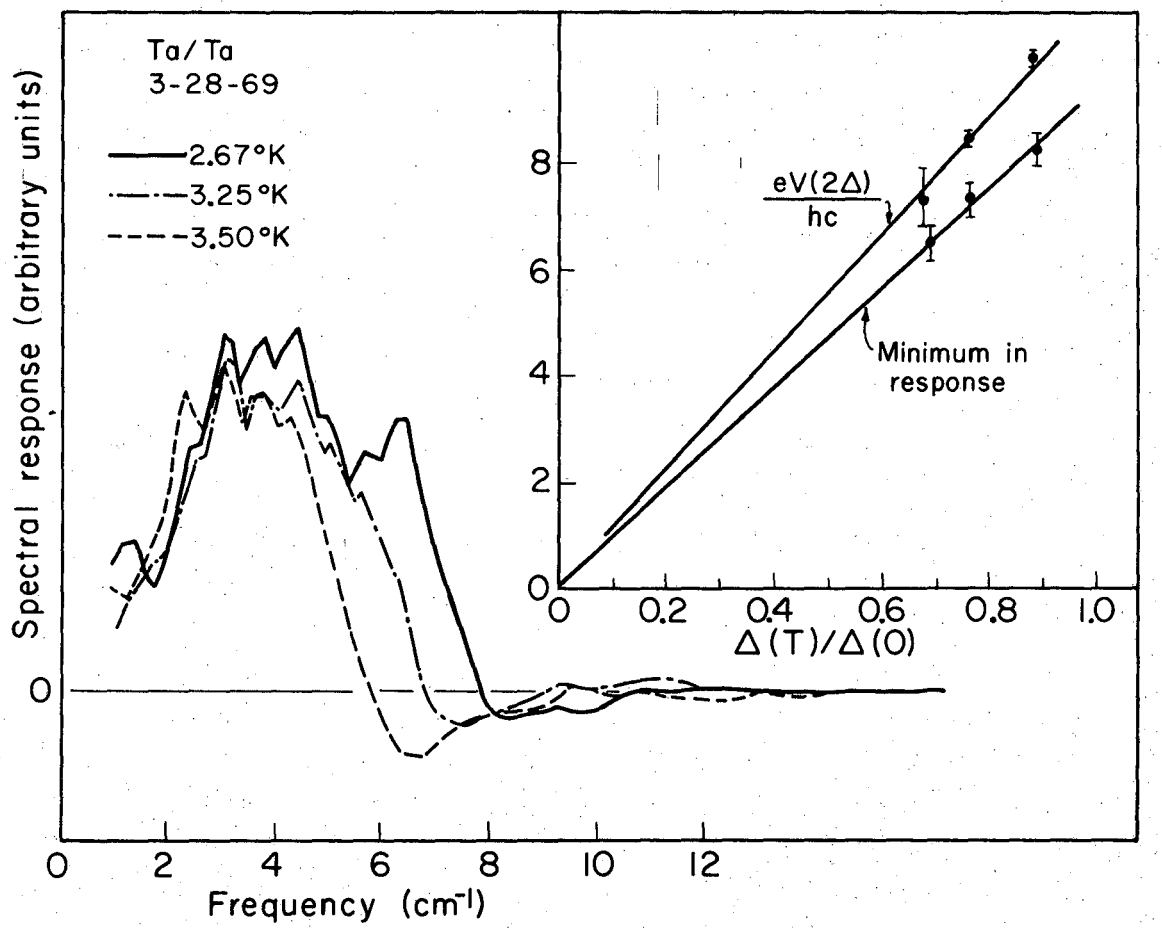

XBL698-3392

Fig. 20

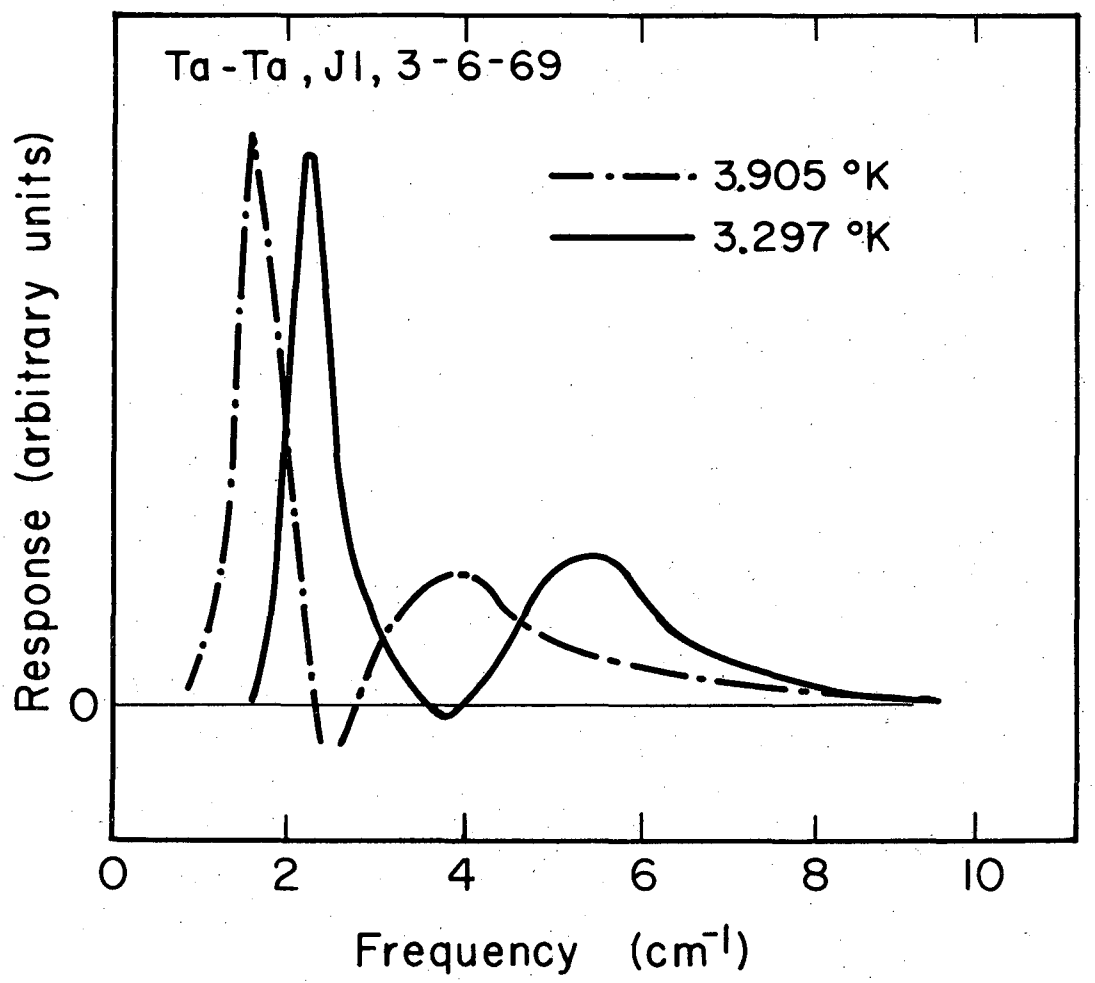

XBL698-3402

Fig. 21

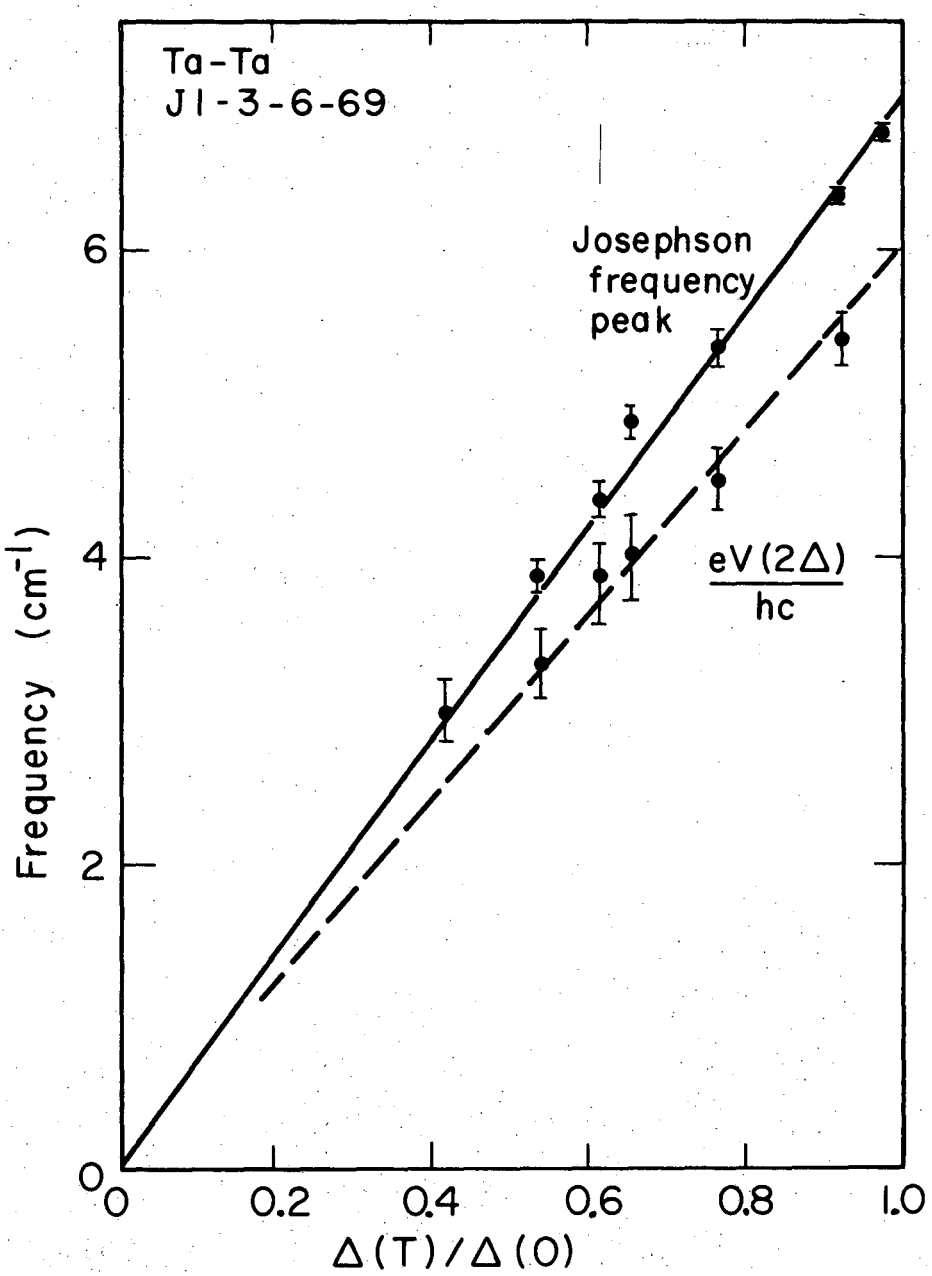

XBL698-3390

Fig. 22

LEGAL NOTICE

This report was prepared as an account of Government sponsored work. Neither the United States, nor the Commission, nor any person acting on behalf of the Commission:

A. Makes any warranty or representation, expressed or implied, with respect to the accuracy, completeness, or usefulness of the information contained in this report, or that the use of any information, apparatus, method, or process disclosed in this report may not infringe privately owned rights; or

B. Assumes any liabilities with respect to the use of, or for damages resulting from the use of any information, apparatus, method, or process disclosed in this report.

As used in the above, "person acting on behalf of the Commission" includes any employee or contractor of the Commission, or employee of such contractor, to the extent that such employee or contractor of the Commission, or employee of such contractor prepares, disseminates, or provides access to, any information pursuant to his employment or contract with the Commission, or his employment with such contractor.

[illegible]
[illegible]
UNIVERSITY OF [illegible]
BERKELEY, CALIFORNIA [illegible]